Published in final edited form as:

Cell Rep. 2024 April 23; 43(4): 113973. doi:10.1016/j.celrep.2024.113973.

The circular RNA *circATP8B(2)* regulates ROS production and antiviral immunity in *Drosophila*

Weihong Liang[1,2], **Wei Liu**[1,2], **Xiao-Peng Xiong**[3], **Jennifer W. Li**[4], **Jian-Liang Li**[3,5], **Ranjan J. Perera**[1,2,3], **Rui Zhou**[1,2,3,6,*]

[1]Departments of Medicine, Biological Chemistry, & Oncology, Johns Hopkins University School of Medicine, Baltimore, MD 21205, USA

[2]Johns Hopkins All Children's Hospital, St. Petersburg, FL 33701, USA

[3]Sanford Burnham Prebys Medical Discovery Institute, La Jolla, CA 92037, USA

[4]Department of Medicine, Brown University, Providence, RI 02912, USA

[5]National Institute of Environmental Health Sciences, Durham, NC 27709, USA

[6]Lead contact

SUMMARY

We identified and validated a collection of circular RNAs (circRNAs) in *Drosophila melanogaster*. We show that depletion of the pro-viral circRNA *circATP8B(2)*, but not its linear siblings, compromises viral infection both in cultured *Drosophila* cells and *in vivo*. In addition, *circATP8B(2)* is enriched in the fly gut, and gut-specific depletion of *circATP8B(2)* attenuates viral replication in an oral infection model. Furthermore, *circATP8B(2)* depletion results in increased levels of reactive oxygen species (ROS) and enhanced expression of dual oxidase (*Duox*), which produces ROS. Genetic and pharmacological manipulations of *circATP8B(2)*-depleted flies that reduce ROS levels rescue the viral replication defects elicited by *circATP8B(2)* depletion. Mechanistically, *circATP8B(2)* associates with Duox, and *circATP8B(2)*-Duox interaction is crucial for *circATP8B(2)*-mediated modulation of Duox activity. In addition, Gαq, a G protein subunit required for optimal Duox activity, acts downstream of *circATP8B(2)*. We conclude that *circATP8B(2)* regulates antiviral defense by modulating *Duox* expression and Duox-dependent ROS production.

In brief

*Correspondence: rzhou13@jhmi.edu.

AUTHOR CONTRIBUTIONS

Conceptualization, W. Liang, W. Liu, X.-P.X., J.W.L., J.-L.L., R.J.P., and RZ.; methodology: W. Liang, W. Liu, X.-P.X., J.W.L., J.-L.L., R.J.P., and RZ.; investigation, W. Liang, W. Liu, X.-P.X., J.W.L., J.-L.L., and RZ.; visualization, W. Liang, W. Liu, X.-P.X., and R.Z.; supervision, R.J.P. and R.Z.; writing – original draft, W. Liang and R.Z.; writing – review & editing, W. Liang, W. Liu, X.-P.X., J.W.L., J.-L.L., R.J.P., and R.Z.

SUPPLEMENTAL INFORMATION

Supplemental information can be found online at https://doi.org/10.1016/j.celrep.2024.113973.

DECLARATION OF INTERESTS

The authors declare no competing interests.

Liang et al. report that depletion of the gut-enriched circular RNA *circATP8B(2)* impairs both systemic and oral infection by RNA viruses in fruit flies. *circATP8B(2)* binds to and inhibits the activity of the ROS-producing enzyme Duox and represses *Duox* expression in the fly gut, thereby regulating Duox-dependent ROS production and antiviral defense.

Graphical Abstract

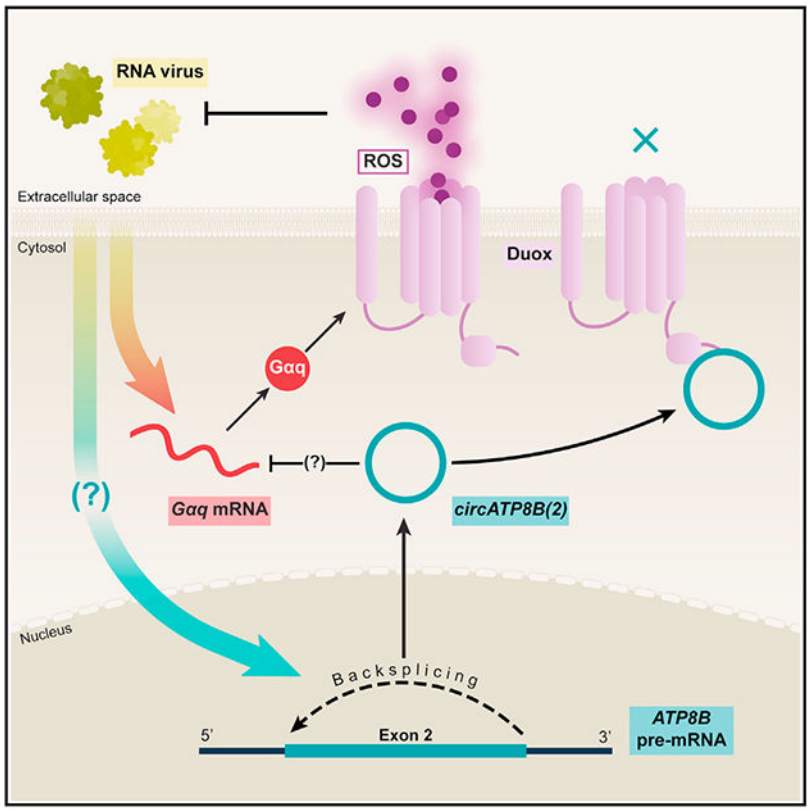

INTRODUCTION

Host organisms have developed powerful defense mechanisms to survive in an environment that contains numerous microbial pathogens and harmful parasites. Insects such as the fruit fly *Drosophila melanogaster* rely exclusively on innate immunity, the first line of defense, against invading pathogens. For example, upon infection by gram-negative bacteria or gram-positive bacteria/fungi, the immune deficiency (IMD) or Toll signaling pathways, respectively, are activated, culminating in the activation of nuclear factor κB (NF-κB)-family transcription factors and production of a battery of potent antimicrobial peptides.[1–5] Upon viral infection, *Drosophila* can mobilize an arsenal of antiviral defense mechanisms with various specificities depending on the identity of viral pathogens as well as the route of infection. For example, in response to systemic infection by a panel of RNA viruses, virus-derived small interfering RNAs (siRNAs) can guide the RNA interference (RNAi) machinery to engage target viral RNAs for destruction.[6–10] In addition, the JAK/STAT (Janus kinase/signal transducer and activator of transcription) signaling pathway plays a key

role in host response against *Drosophila* C virus (DCV) infection.[11] Furthermore, select components of the Toll and IMD signaling pathways have been shown to be involved in antiviral immunity.[12] Moreover, the cyclic guanosine monophosphate (GMP)-AMP synthase (cGAS)-stimulator of interferon genes (STING) pathway detects viral RNA to activate NF-κB-regulated gene expression.[13,14] Last, certain components of RNA degradation and autophagy machineries are required for clearance of infection by select RNA viruses.[15–17]

The aforementioned antiviral mechanisms primarily combat systemic viral infection. In nature, fruit flies feed on decaying food contaminated with microbes. Thus, ingestion of viral pathogens through the digestive tract is a natural route of infection. This triggers a localized antiviral response in the gut, which is distinct from the immune response against systemic infection. For example, mutations in the Toll pathway can cause increased susceptibility to oral but not systemic infection by viral pathogens such as DCV and Flock House virus (FHV).[18] In addition, while RNAi is the major defense mechanism against systemic viral infection, it does not seem to be essential for viral clearance upon oral infection.[19] Last, elevated reactive oxygen species (ROS) levels have been shown to correlate with antiviral protection in *Wolbachia*-infected flies.[20]

Non-coding RNAs (ncRNAs) play a key role in regulating host-virus interactions in eukaryotes. For example, siRNAs can guide the RNAi machinery to target viral RNAs for destruction.[6,7] In addition, microRNAs (miRNAs) can profoundly impact the magnitude and duration of the inflammatory response upon viral infection by targeting mRNAs encoding signaling proteins or inflammatory cytokines.[21–23] Furthermore, select virus-derived ncRNAs, such as Epstein-Barr virus-encoded RNAs (EBERs) and Herpesvirus saimiri U RNAs (HSURs) can modulate the viral life cycle.[24,25] Circular RNAs (circRNAs) are products of “head-to-tail” back-splicing events that have been discovered in diverse eukaryotes and constitute a recent addition to the ncRNA collection.[26,27] circRNAs have been implicated in regulating myriad biological processes, including innate immunity, neurodevelopment, and gene control.[28–32] In particular, select circRNAs can sequester protein kinase R and modulate antiviral defense in mammals.[33]

To investigate the role of circRNAs in antiviral immunity in *Drosophila*, we performed RNA sequencing and identified and validated a collection of circRNAs that display significant changes in expression levels upon viral infection. We show that depletion of *circATP8B(2)*, but not its linear siblings, impairs infection by a panel of RNA viruses in cultured *Drosophila* cells. Similarly, ubiquitous depletion of *circATP8B(2) in vivo* compromises systemic viral infection and enhances host survival. Importantly, restoring *circATP8B(2)* expression in *circATP8B(2)*-depleted cells or flies suppresses these phenotypes. In addition, our analyses reveal that *circATP8B(2)* is enriched in the fly gut and that *circATP8B(2)* expression is induced by oral ingestion of viruses but not bacteria. Furthermore, gut-specific depletion of *circATP8B(2)* leads to enhanced defense against oral viral infection, elevated ROS levels, and upregulation of the ROS-producing enzyme Duox.[34] Mechanistically, *circATP8B(2)* associates with Duox, and such *circATP8B(2)*-Duox interaction is crucial for *circATP8B(2)*-mediated regulation of ROS production. Last, genetic and pharmacological modulations that reduce ROS levels, or depletion of Gaq, a G protein subunit required for optimal Duox activity,[35] suppress the viral infection phenotypes elicited by *circATP8B(2)*

depletion. Thus, our study demonstrates that ROS act as antiviral agents against oral viral infection and that *circATP8B(2)* regulates antiviral immunity, at least in part, by modulating ROS production.

RESULTS

Identification of circRNAs in response to RNA virus infection

To identify circRNAs potentially implicated in host-virus interaction, we extracted total RNA from cultured *Drosophila* Schneider Line 2 (SL2) cells that were either left untreated or infected with FHV. Subsequently, ribosomal RNAs and linear RNAs were removed using the Ribo-zero kit and RNase R, respectively; the resultant circRNA-enriched samples were subjected to RNA sequencing (RNA-seq). Based on the presence of a "back-spliced" exon junction, in which the 3′ end of a downstream exon joins the 5′ end of an upstream exon,[30,36,37] more than 2,000 candidate circRNAs were identified (Data S1). We employed three strategies to validate circRNAs: (1) PCR, where convergent primers amplify products from both genomic DNA and cDNA templates, whereas divergent primers amplify circRNA-derived products exclusively from cDNA (Figures S1A–S1C); (2) Sanger sequencing of the PCR product amplified by divergent primers, which confirms back-spliced exon junctions (Figure S1B); and (3) RNase R treatment, which preferentially degrades linear but spares circRNAs (Figure S1D). Among the 60 candidate circRNAs analyzed (Figure S1E; Data S1), 51 have been validated (Data S1).

Depletion of *circATP8B(2)* compromises viral infection in cultured *Drosophila* cells

To further explore potential involvement of circRNAs in antiviral defense, we designed and stably expressed in *Drosophila* SL2 cells small hairpin RNA (shRNA) constructs (*shRNA-A*) targeting the back-spliced exon junction. Cells were subsequently challenged with FHV, and levels of viral RNA and various circRNAs were examined by RT-PCR. Compared with control knockdown using shRNA targeting *white* (*sh-w*), depletion of 4 pro-viral circRNAs led to a 5- to 7-fold decrease in levels of FHV RNAs without significant impact on cell viability (Figures 1A, 1B, and S2). In addition, we tested two additional RNA viruses, DCV and cricket paralysis virus (CrPV), and observed similar phenotypes (Figures 1A and S2B). Importantly, only circRNAs were depleted by shRNAs, while levels of linear siblings remained unchanged, thereby demonstrating specificity (Figures 1B and 1C). Next, to minimize potential off-target effects, we tested an independent shRNA (*shRNA-B*) and observed similar phenotypes (Figures S3A–S3C). Last, we assessed the impact of depleting linear RNA siblings on viral infection. As expected, depleting the antiviral RNAi factor Ago2 caused an increase in FHV RNA levels (Figures S3D and S3E).[7] In contrast, depleting linear RNA siblings by two independent double-stranded RNAs (dsRNAs), which do not overlap with circRNAs, did not affect FHV RNA levels (Figures S3D and S3E). We conclude that select circRNAs, but not their linear siblings, impact viral infection in cultured *Drosophila* cells.

Consistent with a reduction in viral RNA levels, we detected a concomitant decrease in viral titer for all 3 viruses tested upon depletion of select circRNAs (Figures 1D and S2C). In addition, we performed immunoblotting to measure levels of the FHV B2 protein.[38]

Among the 4 circRNAs tested, only depletion of *circATP8B(2)* caused a consistent reduction in FHV B2 protein levels (Figures 1E and 1F). It is unclear why depleting the other three circRNAs did not consistently affect viral protein levels. We therefore focused on *circATP8B(2)* (Figure S1B) for further analysis because its depletion consistently impacted levels of viral RNA, protein, and titer.

Next, we expressed a combination of constructs for *circATP8B(2)*, empty vector (control), *sh-circATP8B(2)*, and the control shRNA (*sh-w*) in SL2 cells, infected cells with FHV, and measured viral RNA levels. Consistent with Figures 1A and S2B, depleting *circATP8B(2)* led to a reduction in FHV RNA levels (Figures 1G, 1H, and S2D). Importantly, while *circATP8B(2)* overexpression in control cells did not affect FHV RNA levels, restoring *circATP8B(2)* expression in *circATP8B(2)*-depleted cells suppressed the FHV viral RNA replication phenotype (Figures 1G, 1H, and S2D). We note that exogenous *circATP8B(2)* carries back-spliced exon junction sequences derived from the vector, which differs from those in endogenous *circATP8B(2)*. Therefore, exogenous *circATP8B(2)* is resistant to shRNA-mediated knockdown (Figure 1H). Importantly, levels of the linear *ATP8B* transcript remained unchanged (Figure 1I). We conclude that *circATP8B(2)*, but not linear *ATP8B*, affects viral infection in cells.

Depletion of *circATP8B(2)* impacts host-virus interaction *in vivo*

To determine whether *circATP8B(2)* affects viral infection *in vivo*, we generated flies carrying *circATP8B(2)* or *sh-circATP8B(2)* transgenes under the control of an upstream activating sequence (UAS). We first crossed various combinations of *sh-circATP8B(2)*, *sh-GFP* (control), *circATP8B(2)*, and empty vector (control) transgenes with flies carrying the ubiquitously expressed *Actin-Gal4* (*Act-Gal4*) driver. Female progeny was injected with RNA viruses (FHV, DCV, and CrPV), and levels of various RNAs were measured. As expected, *circATP8B(2)* was efficiently depleted in *Act>sh-circATP8B(2)* animals, while levels of linear *ATP8B* remained unchanged (Figures 2A and 2B). Reminiscent of the observations made in SL2 cells, ubiquitous depletion of *circATP8B(2) in vivo* caused a significant reduction in levels of viral RNAs. Restoring *circATP8B(2)* expression rescued this phenotype (Figures 2C–2E and S4). Male progeny displayed similar phenotypes (Figure S5). In addition, we generated and analyzed a second *sh-circATP8B(2)* transgene, and similar phenotypes were observed (Figure S6A). Next, we depleted linear *ATP8B* by expressing the *sh-ATP8B* transgene driven by *Act-Gal4* and assessed the impact on FHV infection. Reminiscent of the observations made in SL2 cells, viral RNA levels were not affected by linear *ATP8B* depletion (Figure S6B). Last, we examined the impact of *circATP8B(2)* depletion on host survival after viral infection. Flies of appropriate genotypes were injected with 3 distinct RNA viruses or sterile PBS (control), and survival was monitored (Figures 2F–2I). While there was no difference in fly survival after PBS injection, *Act>sh-circATP8B(2)* flies succumbed to viral challenges at a later time than the *Act>sh-GFP* control animals, consistent with a reduction in viral RNA levels upon *circATP8B(2)* depletion (Figures 2F–2I). In addition, restoring *circATP8B(2)* expression in *Act>sh-circATP8B(2)* animals rescued this phenotype (Figures 2F–2H). Thus, our data demonstrate that *circATP8B(2)*, but not its linear siblings, regulates antiviral defense against systemic infection *in vivo*.

circATP8B(2) is enriched in the gut and impacts defense against oral infection

To identify potential effector genes that act downstream of *circATP8B(2)* to impact antiviral defense, we performed RNA-seq and compared the RNA expression profile of *Act>sh-circATP8B(2)* flies with that of *Act>sh-GFP* control animals. In total, 139 transcripts displayed significant changes in expression upon *circATP8B(2)* depletion both in males and females (Figures S7A and S7B; Data S1). The significantly changed genes were grouped into 11 categories based on their predicted/validated roles (Figure S7C). Notably, genes that are highly expressed in the gut, such as *LysB*, *LysC*, *LysD*, and *IRC*, as well as several Neprilysin-like metallopeptidases (*NEPL*) genes, were among the up-regulated genes (Figures S7D and S7E; Data S1).

Next, we analyzed the *circATP8B(2)* expression pattern *in vivo*. We found that *circATP8B(2)*, but not its linear siblings, was prominently enriched in both the adult and larval gut. Levels *circATP8B(2)* were 3- to 5-fold higher in the adult fly gut than in carcasses with the gut removed and ~70-fold higher in the larval gut than in whole larvae (Figure 3A and 3C). In contrast, the linear *ATP8B* transcripts were evenly distributed across various adult/larval tissues (Figure 3B and 3D).

The prominent enrichment of *circATP8B(2)* in the fly gut and the observation that select gut-enriched genes (such as those involved in digestion and metabolic processes) are up-regulated upon *circATP8B(2)* depletion implies that *circATP8B(2)* might impact antiviral immunity in the gastrointestinal (GI) tract. Therefore, we employed an oral infection model to assess the impact of *circATP8B(2)* depletion on antiviral defense. We first expressed various combinations of *sh-circATP8B(2)*, *sh-GFP* (control), *circATP8B(2)*, and empty vector (control) transgenes under the control of the gut-specific driver *Myo1A-Gal4*. Male and female progenies were fed with food supplemented with various RNA viruses, and fly gut tissue was harvested 24 h and 48 h post infection. We found that depletion of *circATP8B(2)* specifically in the gut led to a reduction in levels of all three viral RNAs and that restoring *circATP8B(2)* expression in *circATP8B(2)*-depleted gut cells rescued these phenotypes (Figures 3E–3H, S8, and S9). In addition, a second *sh-circATP8B(2)* transgene yielded similar phenotypes (Figure S6C). In contrast, depleting linear *ATP8B* in the gut did not affect viral RNA levels (Figure S6D). We also reared flies on food supplemented with antibiotics and detected no changes in the phenotypes (Figure S10). In addition, our flies tested negative for *Drosophila* A virus (DAV) and Nora virus (cycle threshold [Ct] >40), suggesting that the gut microbiome or infection by DAV or Nora virus was not responsible for the viral RNA replication phenotype in our flies. Furthermore, reminiscent of the phenotypes of flies with gut-specific depletion of *circATP8B(2)*, flies with ubiquitous depletion of *circATP8B(2)* displayed a similar reduction in viral RNA levels upon oral infection (Figure S11). Moreover, select SNPs at the *pastrel* locus impact resistance to viral infection in flies.[39] All flies in the ubiquitous *circATP8B(2)* knockdown experiments carry identical SNPs (Data S1). Considering that *Act>sh-circATP8B(2)* animals display enhanced antiviral defense in both systemic and oral infection models, and that *circATP8B(2)* depletion in cultured SL2 cells causes a similar phenotype, it is unlikely that enhanced antiviral defense upon *circATP8B(2)* depletion is due to differences in SNP genotype at the *pastrel* locus.

Last, we assessed host survival up to 45 days after oral infection. No difference was found between control flies and flies with gut-specific silencing of *circATP8B(2)* (Figure S12). Our findings are consistent with a recent study showing that oral infections in adult flies are ultimately cleared in wild-type flies and cause very little mortality.[19] Thus, it would be challenging to detect any enhancement in survival upon oral viral infection in flies with gut-specific depletion of *circATP8B(2)*. We conclude that *circATP8B(2)* is enriched in the gut and impacts antiviral defense *in vivo* against oral infection.

Depletion of *circATP8B(2)* in the fly gut results in elevated levels of ROS

Select components of RNAi and IMD signaling have been implicated in antiviral defense.[6,7,40] Our analysis did not reveal any significant changes in expression levels of genes encoding components and/or targets of IMD signaling and RNAi upon *circATP8B(2)* depletion in the gut (Figure S13). ROS are components of the host defense against bacterial and fungal infection in the gut.[34,41] Considering that (1) *circATP8B(2)* is enriched in the fly gut and that (2) genes encoding digestive enzymes, components of select metabolic pathways, and the ROS-removing enzyme IRC (immune-regulated catalase) displayed significant changes in expression levels upon *circATP8B(2)* depletion (Figures S7C and S7D), we set out to examine whether ROS levels in the fly gut are affected by *circATP8B(2)* depletion. Flies of appropriate genotypes were fed with food supplemented with PBS or DCV, and ROS levels in the fly gut were measured. We found that oral DCV infection caused an increase in ROS levels in the gut (Figure 4A). Importantly, we detected elevated levels of ROS in the *circATP8B(2)*-depleted fly gut compared with control samples. In addition, restoring *circATP8B(2)* expression in *circATP8B(2)*-depleted flies rescued this phenotype (Figure 4A). Similar phenotypes were observed in flies reared on food supplemented with antibiotics, suggesting that the gut microbiome does not affect this phenotype (Figure S14A). Besides measuring ROS levels, we performed an immunofluorescence assay using antibodies against 4-hydroxynonenal (4-HNE), an α,β-unsaturated hydroxyalkenal and a product of ROS-mediated lipid peroxidation.[42] Reminiscent of increased ROS levels detected in *circATP8B(2)*-depleted flies, we found that 4-HNE signals in the *Myo1A>sh-circATP8B(2)* fly gut were significantly higher than in control samples and that restoring *circATP8B(2)* expression rescued this phenotype (Figures 4B and 4C). Oral infection by DCV also led to an increase in 4-HNE levels (Figures 4B and 4C). However, no difference was found between the *circATP8B(2)*-depleted fly gut and control samples after DCV infection, possibly due to differences in sensitivity of the 4-HNE and ROS assays. Alternatively, 4-HNE levels might have reached saturation after DCV infection. Nonetheless, these orthogonal analyses show that *circATP8B(2)* depletion in the fly gut leads to elevated ROS levels, at least under baseline conditions. Furthermore, to establish the functional relevance of increased ROS levels elicited by *circATP8B(2)* depletion, we fed flies with food supplemented with the bacterial pathogen *Ecc15* and measured bacterial load in the fly gut.[43] Our analysis revealed an inverse correlation between ROS levels and bacterial load (Figures 4A–4D), consistent with previous reports showing that ROS are antimicrobial agents.[34,41] *Wolbachia* infection has been shown to affect ROS levels and antiviral defense in *Drosophila*.[20] Our flies tested negative for *Wolbachia* (Figure S15), ruling out involvement of *Wolbachia*.

Next, we measured levels of *Duox* mRNA, which encodes a ROS-producing enzyme implicated in microbial clearance in the gut.[34,41] Oral infection by DCV led to an increase in levels of *Duox* mRNA (Figures 4E and S14B). Notably, correlating with elevated ROS levels elicited by *circATP8B(2)* depletion, we detected higher levels of *Duox* transcript in the *Myo1A>sh-circATP8B(2)* fly gut than in control samples (Figures 4E and S14B). In addition, restoring *circATP8B(2)* expression in the *circATP8B(2)*-depleted fly gut reduced *Duox* expression to levels comparable with those detected in controls (Figures 4E and S14B). Furthermore, we performed an immunofluorescence assay using anti-Duox antibodies and found that levels of Duox protein followed the same pattern as *Duox* RNA (Figures 4F and 4G). Similar observations were made in SL2 cells (Figure S16). We conclude that depletion of *circATP8B(2)* leads to elevated expression of *Duox* and an increase in ROS levels.

Elevated ROS levels correlate with impaired viral infection in *circATP8B(2)*-depleted flies

To examine whether elevated levels of ROS in the *circATP8B(2)*-depleted fly gut are underlying the compromised viral infection phenotype, we employed two independent strategies to reduce ROS levels and examined the impact on viral infection: (1) depleting *Duox* using two independent shRNA transgenes and (2) feeding flies with the ROS inhibitor N-acetyl-l-cysteine (NAC) prior to viral infection.[44] As expected, depletion of *Duox* or feeding with NAC was sufficient to reduce ROS levels in control animals (Figures 5A, 5C, S17A, and S17C), leading to increased viral RNA load (Figures 5B–5D, S17B, and S17D). In particular, these genetic and pharmacological manipulations in *circATP8B(2)* knockdown animals led to a reduction in ROS levels that was comparable with controls, accompanied by restoration of viral RNA load (Figures 5 and S17). Taken together, our data demonstrate that ROS are antimicrobial agents that impair viral infection in *circATP8B(2)*-depleted flies.

circATP8B(2) associates with Duox and modulates ROS production

Previous studies show that select circRNAs associate with miRNAs and impact miRNA levels and/or function,[28,30,45] encode functional proteins,[31,32,46,47] or directly interact with proteins.[47,48] To gain insight into the mechanism underlying *circATP8B(2)* function, we first tested the miRNA-binding and protein-coding hypotheses by performing AGO1 and ribosomal protein RpL22 RNA immunoprecipitation (RIP), respectively. We noticed that, while *circATP8B(2)* harbors a putative open reading frame (ORF), no enrichment of *circATP8B(2)* was detected in the RpL22 pulldown sample compared with the control (Figure S18). In addition, expressing a *circATP8B(2)* transgene containing a 3×FLAG epitope immediately upstream of the stop codon in the *circATP8B(2)* ORF failed to yield FLAG-tagged proteins in SL2 cells. Thus, it is unlikely that *circATP8B(2)* encodes proteins. Furthermore, we found that *circATP8B(2)* was enriched in the AGO1 complex, implying potential *circATP8B(2)*-miRNA interactions (Figure S18). However, a thorough survey of *circATP8B(2)* revealed no significant enrichment of binding sites for seed sequences shared by any miRNA families, suggesting that such *circATP8B(2)*-miRNA binding is unlikely to impact the function of any miRNA families. Last, functional miRNA-binding sites can be located within the ORF of target mRNAs.[49] Since *circATP8B(2)* is derived from a single exon within the *ATP8B* ORF, even if *circATP8B(2)* associates with miRNAs, it is unclear

whether such *circATP8B(2)*-miRNA binding is specific to *circATP8B(2)*, linear *ATP8B*, or both.

Next, we purified *circATP8B(2)*-containing complexes from SL2 cells using a biotinylated oligo probe complementary to the back-spliced exon junction of *circATP8B(2)* (Figure S19A). We found that *circATP8B(2)* was efficiently pulled down by this probe but not by a control probe with a sense sequence to the back-spliced exon junction of *circATP8B(2)* (Figure S19B). Subsequent mass spectrometry analysis identified candidate *circATP8B(2)*-associated proteins (Data S1). To validate *circATP8B(2)*-protein interaction, we expressed select FLAG-tagged proteins (Pebp1, $Duox_{1219–1537}$, and EndoG) and the control protein Ran together with *circATP8B(2)* in SL2 cells. The *circATP8B(2)*-protein complexes were purified using the aforementioned biotinylated oligo probe and subjected to immunoblot using anti-FLAG antibodies. Our analysis revealed that Pebp1 and $Duox_{1219–1537}$, but not endoG or the control protein Ran, were present in the *circATP8B(2)* complex (Figure S19C), suggesting that Pebp1 and Duox, but not EndoG, associate with *circATP8B(2)*. In a reciprocal RIP assay, various FLAG-tagged proteins were expressed in SL2 cells and purified using anti-FLAG antibody, and levels of *circATP8B(2)* in immunopurified complexes were measured (Figure S19D). Consistent with the results from the affinity purification assay using *circATP8B(2)* as bait, we detected higher levels of *circATP8B(2)* in Pebp1 and $Duox_{1219–1537}$ pull-down samples than in the control sample Ran, whereas comparable background levels of the control *Rp49* were detected in all samples (Figures S19E and S19F). We conclude that *circATP8B(2)* interacts with Pebp1 and Duox.

The C-terminal region of Duox harbors a FAD (flavin adenine dinucleotide)-binding domain (FAD-BD) and NAD (nicotinamide adenine dinucleotide)-binding domain (NAD-BD) (Figure 6A). To identify protein domain(s) responsible for interaction with *circATP8B(2)*, we first expressed FLAG-tagged Duox FAD-BD, NAD-BD, or the control protein Ran in SL2 cells and examined whether they can pull down *circATP8B(2)*. We detected higher levels of *circATP8B(2)* in the NAD-BD, but not the FAD-BD pull-down, than in the control sample Ran (Figures 6B and 6C). In contrast, comparable background levels of the control *Rp49* were detected in all samples (Figure 6D). Next, we expressed *circATP8B(2)* together with various FLAG-tagged Duox fragments or the control protein Ran, then affinity-purified and analyzed the *circATP8B(2)*-containing complex by immunoblot. Our analysis revealed that the Duox NAD-BD, but not the FAD-BD or the control protein Ran, was present in the *circATP8B(2)* complex (Figures 6E and 6F). We conclude that the NAD-BD of Duox is sufficient for interaction with *circATP8B(2)*.

To identify the *circATP8B(2)* region required for interaction with Duox, we expressed, in SL2 cells, full-length or various *circATP8B(2)* mutants carrying internal deletions and assessed their interactions with Duox. All *circATP8B(2)* mutants missing fragments encompassing nucleotides 50–122 failed to pull down the Duox NAD-BD (Figure 6F). In contrast, *circATP8B(2)* mutants carrying smaller deletions (Δ50–82, Δ67–82, or Δ17–41) retained interaction with the Duox NAD-BD (Figure 6G). As a negative control, no NAD-BD was detected in a parallel purification using a probe with sense sequence to the back-spliced exon junction of *circATP8B(2)* (Figure 6G). Interestingly, M-fold analysis indicates that *circATP8B(2)* may adopt an extensive hairpin structure, which is disrupted in

mutants lacking nucleotides 50–122 (Figure S20), suggesting that such a motif is required for *circATP8B(2)*-Duox interaction.[50] Last, to assess the functional relevance of such an interaction, we expressed full-length or various *circATP8B(2)* mutants in *circATP8B(2)*-depleted SL2 cells and examined the impact on ROS levels. Reminiscent of the observations made *in vivo*, depletion of *circATP8B(2)* in SL2 led to elevated ROS levels (Figure 6H). In addition, restoring expression of full-length *circATP8B(2)* in *circATP8B(2)*-depleted cells was sufficient to achieve a reduction in ROS levels that was similar to those in controls. Importantly, such a rescue effect depends on *circATP8B(2)*-Duox interaction; only *circATP8B(2)* mutants that retained interaction with Duox (Δ50–82, Δ67–82, or Δ17–41), but not Δ50–122, which failed to interact with Duox, could reduce ROS levels. The degree of rescue effect appeared to correlate with the strength of interaction between Duox and various *circATP8B(2)* mutants (Figures 6G and 6H). We conclude that *circATP8B(2)*-Duox interaction is crucial for *circATP8B(2)*-mediated regulation of ROS production.

Gαq acts downstream of *circATP8B(2)* to regulate the Duox activity pathway

Gαq is a G protein subunit implicated in regulating Duox activity.[35] *Gαq* mRNA levels were upregulated in the fly gut upon DCV infection. In addition, levels of the *Gαq* transcript were elevated in the *Myo1A>circATP8B(2)* fly gut compared with controls. Restoring *circATP8B(2)* expression in *circATP8B(2)*-depleted flies rescued this phenotype (Figure 7A). We found that depletion of *Gαq* by two independent dsRNAs in control (*sh-w*) cells led to a 2-fold increase in levels of DCV RNA, suggesting that Gαq is involved in controlling viral RNA replication. Importantly, while *circATP8B(2)*-depleted cells displayed a significant reduction (~10-fold) in viral RNA levels, depletion of *Gαq* in these cells led to a marked rescue of this phenotype by restoring viral RNA levels to ~40%–120% of those detected in control samples (Figure 7B). Notably, levels of Duox RNA were not affected by *Gαq* depletion (Figure 7C), implying that Gαq is involved in regulating Duox activity but not expression. To further confirm these findings *in vivo*, we depleted *Gαq* using two independent shRNA transgenes in the fly gut, fed flies with DCV, and examined the impact on levels of DCV RNA and ROS. Reminiscent of the phenotype observed in SL2 cells, *Gαq* depletion is sufficient to cause a reduction in ROS levels in control animals (Figure 7D), correlating with a marked increase in viral RNA load (Figure 7E). Importantly, knocking down *Gαq* in *circATP8B(2)*-depleted flies led to a reduction in ROS levels that was similar to those detected in control animals and a significant restoration in viral RNA load (Figures 7D and 7E). In addition, levels of *Duox* RNA remained unaffected upon *Gαq* depletion (Figure 7F). We conclude that Gαq acts downstream of *circATP8B(2)* to regulate ROS production by modulating Duox activity but not expression.

In summary, our study identifies the gut-enriched *circATP8B(2)* as a regulator of ROS production and antiviral defense in *Drosophila*. We show that *circATP8B(2)* is upregulated upon viral infection, and that depleting *circATP8B(2)*, either in cells or *in vivo*, leads to an upregulation of *Duox* expression and elevated ROS levels that correlates with a decrease in viral RNA load. In addition, while *circATP8B(2)*-depleted flies display elevated ROS levels and a reduction in viral RNA load, genetic or pharmacological manipulations in *circATP8B(2)*-depleted flies resulted in a marked rescue of such phenotypes, suggesting that ROS are antimicrobial agents that underlie the enhanced antiviral defense phenotype

in *circATP8B(2)*-depleted flies. Furthermore, our analysis reveals that *circATP8B(2)* associates with the NAD-BD of Duox and that *circATP8B(2)*-Duox interaction is crucial for *circATP8B(2)*-mediated regulation of ROS production and antiviral defense. Last, we show that Gαq acts downstream of *circATP8B(2)* to regulate Duox activity (Figure 7G). Thus, our study provides evidence showing that ROS plays a key role in antiviral immunity in an oral infection model and identifies and characterizes the gut-enriched *circATP8B(2)* as a regulator of Duox-dependent ROS production and antiviral defense.

DISCUSSION

In this study, we show that the gut-enriched circRNA *circATP8B(2)* regulates ROS production. While *circATP8B(2)*-depleted flies display elevated levels of ROS that correlate with enhanced antiviral defense, genetic and pharmacological manipulations that bring ROS levels back to those observed in control animals can rescue such a viral infection phenotype (Figures 4, 5, and S17). These observations strongly suggest that ROS are key effector molecules that act downstream of *circATP8B(2)* to modulate antiviral defense. ROS are potent broad-spectrum antimicrobial agents that can eliminate bacteria or fungi by damaging DNA, RNA, and proteins and promote oxidative degradation of lipids in cell membranes. It is conceivable that similar processes take place in antiviral defense. Alternatively, ROS could affect the activity of downstream signaling pathways and/or the production of additional effector molecules that, in turn, modulate viral infection. It is currently unclear whether either or both mutually non-exclusive modes of action underlie the antiviral effect of ROS.

Our study shows that *circATP8B(2)* impacts both the expression and activity of Duox. In particular, depleting *circATP8B(2)*, either in cultured cells or in the fly gut, leads to an increase in levels of both *Duox* transcript and protein that correlate with elevated levels of ROS. Interestingly, levels of *IRC*, which encodes a ROS-removing enzyme,[41] are also elevated upon *circATP8B(2)* depletion (Figure S21A). Similarly, viral infection in SL2 cells and/or *in vivo* causes upregulation of both *Duox* and *IRC* (Figures S7D and S21A), suggesting that ROS levels are under tight regulation. On the one hand, elevated ROS levels are beneficial for optimal antiviral defense; on the other hand, excessive ROS can cause oxidative stress and compromise cellular function. Interestingly, *circATP8B(2)* is upregulated by viral infection but not by bacterial infection or alterations in redox status (Figure S21B). In contrast, levels of linear *ATP8B* remain unchanged, indicating that viral infection promotes back-splicing, but not transcription, at the *ATP8B* locus (Figure S21C). The exact molecular cue(s) responsible for viral infection-mediated upregulation of *circATP8B(2)* biogenesis are currently unclear. Nonetheless, our data suggest that proper control of *circATP8B(2)* expression is part of the *Drosophila* antiviral defense mechanism necessary for achieving both effective antiviral defense and appropriate maintenance of redox balance.

Our data reveal that *circATP8B(2)* associates with the NAD-BD of Duox (Figures 6A–6D). It is currently unclear whether such a binding event confers a conformational change in Duox, thereby impacting its enzymatic activity. Nonetheless, considering that select metabolic enzymes can potentially bind RNAs,[51] it is tantalizing to speculate that

RNA binding may be a potential mechanism for regulating enzymatic activities. We note that reciprocal RIP assays do not demonstrate direct *circATP8B(2)*-Duox interaction, as additional protein(s) could mediate such an interaction. Nonetheless, our study shows that such a *circATP8B(2)*-Duox interaction is necessary for *circATP8B(2)*-dependent regulation of Duox activity (Figures 6, S19, and S20). In addition, *circATP8B(2)* impacts *Gaq* expression, which is required for optimal Duox activity (Figure 7A). Furthermore, *circATP8B(2)* also affects *Duox* expression (Figures 4E–4G, S16A, S16B, and S16E). Thus, it appears that *circATP8B(2)* modulates ROS production via at least three independent mechanisms that converge on Duox. It is currently unclear whether there is a hierarchy among these mechanisms in various cell types. Alternatively, the aforementioned modes of action could operate in a concerted manner to achieve optimal control of ROS production and robust antiviral defense. Interestingly, while *circATP8B(2)* depletion led to elevated levels of ROS and impaired viral infection, overexpression of *circATP8B(2)* had no obvious impact (Figures 1G, 1H, 2, 3E–3H, 4, and S16). Considering that *circATP8B(2)* associates with Duox and inhibits Duox activity (Figures 6 and S19), it is possible that endogenous Duox is limiting under baseline conditions. In this scenario, endogenous *circATP8B(2)* is sufficient to achieve robust inhibition of expression and/or activity of Duox, and supplementing exogenous *circATP8B(2)* may not boost such inhibitory effects.

Last, while our analyses reveal that *circATP8B(2)* is enriched in the fly gut and that depletion of *circATP8B(2)*, either ubiquitously or specifically in gut cells, enhances antiviral defense in an oral infection model, ubiquitous depletion of *circATP8B(2)* throughout the fly body compromises viral RNA replication and enhances host survival upon systemic infection (Figures 2, 3, and S11). These observations suggest that *circATP8B(2)* not only operates in the fly gut to combat oral viral infection but also acts in other cells/tissues to achieve optimal defense against systemic infection.

In summary, our study identifies *circATP8B(2)* as a modulator of ROS production and antiviral defense in cultured cells and *in vivo* by impacting the expression and activity of *Duox*: (1) *circATP8B(2)* associates with Duox and inhibits Duox activity; (2) *circATP8B(2)* impacts the expression of Gaq, which is required for optimal Duox activity; and (3) *circATP8B(2)* regulates *Duox* expression. Our study highlights a key role of ROS in antiviral defense, provides evidence that select circRNAs regulate antiviral immunity, and reveals mechanistic insights into the mechanism underlying the regulation of protein activity by RNAs.

Limitations of this study

We employed a shRNA-mediated knockdown model, but not null mutants, to investigate *circATP8B(2)* function. In addition, the mechanism underlying viral infection-induced upregulation of *circATP8B(2)* is unclear.

STAR★METHODS

RESOURCE AVAILABILITY

Lead contact—Further information and requests for resources and reagents should be direct to and will be fulfilled by the lead contact, Rui Zhou (rzhou13@jhmi.edu).

Materials availability—Unique materials generated in this study are available upon request: lead contact, Rui Zhou (rzhou13@jhmi.edu).

Data and code availability

- This paper generated RNA-seq data. The dataset is available from Gene Expression Omnibus (GSE248667). These accession numbers for the datasets are listed in the key resources table.
- This paper does not report original code.
- Any additional information required to reanalyze the data reported in this work paper is available from the lead contact upon request.

EXPERIMENTAL MODEL AND STUDY PARTICIPANT DETAILS

Drosophila melanogaster—All fly stocks used are Wolbachia free and listed in the key resource table. Flies were maintained on standard molasses food at room temperature. Flies (4–7 days old) of the indicated genotype were used. Siblings were randomly sorted into experimental groups.

Cell culture—SL2 were cultured in Schneider's medium (Invitrogen-GIBCO, Carlsbad, CA) supplemented with 10% heat-inactivated fetal bovine serum (Hyclone), 100 U/mL of penicillin, and 100 μg/mL streptomycin (Invitrogen-GIBCO, Carlsbad, CA) at 25 °C.

Virus generation—DCV, FHV and CrPV were propagated by infecting *Drosophila* cells maintained at 25 °C and collecting cells and supernatant after 75% of cells had died. Infected cells and supernatant were then subject to ultracentrifugation steps and resuspended in PBS.

METHOD DETAILS

Circular RNA identification—Circular RNA identification was conducted following the methodology outlined in a previous publication.[32] In brief, the raw reads (fastq files) underwent pre-processing, involving the trimming of adapter sequences and the exclusion of low-quality reads (defined as reads with average base quality of ≤20). Circular RNA detection was based on the computational pipeline.[28,57] The raw reads, which were paired-end (2x100), were aligned to the *Drosophila* reference genome (dm3) using bowtie2 (version 2.2.5).[53] The find_circ program (version 1.0), employing the parameters recommended by the developer, was then applied to detect circRNAs using the unmapped reads.[28]

RNA-seq data analysis—Adaptor sequences and low-quality reads (those with an average quality score <20) were removed from the paired-end raw data using Trim-galore

(version 0.4.4). The resulting cleaned reads were aligned to the Drosophila melanogaster (dm6) reference genome using the STAR splice-aware aligner (version 2.6.0c) with default parameters.[54] Ambiguous reads mapping to multiple regions in the genome and reads with a MAPQ score less than 10 were discarded. Subread featureCounts (version 2.0.1) was then utilized for gene quantification,[55] employing the FlyBase r6.40 gene annotation. Genes without read counts in all samples were excluded from subsequent analysis. The remaining genes analyzed by the edgeR package to identify differential expression between control and treated samples.[56] Benjamini and Hochberg's method was applied to control the false discovery rate. Genes were considered significantly differentially expressed if they met the following criteria: detected in at least one sample (RPKM >1), fold change exceeding 2, and an adjusted p value less than 0.05.

DNA constructs—To knock down the circRNAs, shRNA constructs were generated using the Valium 20 parental vector.[31,32] Briefly, DNA fragments containing the designed shRNA sequences were amplified by PCR and cloned into Valium 20 using NheI and EcoRI. To overexpress *circATP8B(2)* in SL2 cells, DNA fragment containing the circATP8B(2)-generating exon was amplified by PCR, and cloned into the Hy_pMT Laccase2 MCS exon vector using NheI and KpnI.[52] To generate deletional mutants of *circATP8B(2)*, DNA fragments were PCR amplified using appropriate divergent oligo pairs that are pre-phosphorylated and the *Hy_pMT Laccase2_ circATP8B(2)* plasmid as template. The resultant PCR product was subsequently treated with Dpn I, ligated using T4 DNA ligase and transformed into competent *E. coli* cells. Mutations were verified by Sanger Sequencing. To generate expression constructs for full-length or various truncational mutants of *circATP8B(2) in vivo*, various versions of the corresponding *Hy_pMT Laccase2_ circATP8B(2)* constructs were digested with XhoI, treated with T4 DNA polymerase, and subsequently digested with NotI to release the *circATP8B(2)* insert. Similarly, the pUAST construct was digested with EcoRI, treated with T4 DNA polymerase and subsequently digested with NotI to release the vector backbone. Subsequently ligation reaction was setup and transformed into competent *E. coli* cells. Resultant constructs were verified by Sanger Sequencing. To generate pMT-Flag-Duox expression constructs, various DNA fragments containing coding sequences for the corresponding Flag-tagged C-terminal fragments of Duox were amplified by PCR and cloned into pRmHa-3 using EcoRI and SalI sites.

RNA extraction and RT-qPCR—For flies infected with viruses via infection, 5 flies were collected for each sample. For flies infected with viruses via oral feeding, 10 fly guts were collected for each sample. At least three independent biological replicates were collected for each experiment. Total RNA was extracted with TRIzol from either flies or cultured SL2 cells. RNA samples were reverse transcribed using Superscript III (Invitrogen, 18080044). Real-time RT-PCR analysis was performed using the SYBR Green PCR master mix (BioRad, 1725275). Relative mRNA levels were calculated by normalization against the endogenous *RP49* mRNA. Fold changes in RNA levels were calculated using the ΔΔCt method. Oligonucleotides used in this assay are listed in Data S1.

***Drosophila* genetics—**Flies were maintained at room temperature with standard fly food. In experiments involving flies reared in antibiotics-containing food, standard fly

food was supplemented with antibiotics (100 μg/mL each of ampicillin, kanamycin and doxycycline). UAS-sh-*circATP8B(2)* transgenic flies were generated using the Valium 20-*circATP8B(2)* construct that integrated into the Attp2 site on the 3rd chromosome (Bestgene). pUAST-*circATP8B(2)* or the control pUAST-Laccase2 MCS exon vector transgenic flies were generated using the corresponding pUAST constructs (Bestgene). To generate *circATP8B(2)* depletion or overexpression flies, *UAS-sh-circATP8B(2)* or pUAST-*circATP8B(2)* transgenic lines were crossed with the *Act-Gal4 or Myo1A-Gal4* driver flies. Control cross was set up using a *UAS-sh-GFP* or *pUAST-Laccase2 MCS exon vector* transgenic flies. All the genotypes of flies used in this study are listed in Data S1.

Cell culture, RNAi and virus infection—S2 cells were cultured at room temperature in Schneider insect cell culture medium (Sigma-Aldrich, S0146) supplemented with 10% fetal bovine serum (HyClone, SH30071.03) and 1% penicillin-streptomycin (Gibco, 15140122) and Glutamax (Gibco, 35050061). Double stranded RNAs (dsRNAs) were generated using 5X MEGAscript T7 Kit.[58] RNAi assays were carried out as the following.[59,60] Essentially, SL2 cells were suspended in serum-free media at the density of $3X10^6$ cells/mL. Subsequently cells were plated into 6-wells plate (~1.5 mL cell suspension per well) and incubated with 10 μg dsRNA. One hour later, 3 mL of FBS-containing complete media were added and cells were incubated for an additional 3 days at room temperature. Cells were subsequently infected by FHV (MOI 0.1) for indicated times, total RNA was extracted from cells and analyzed by qPCR. To deplete or overexpress circRNAs, transfection was performed in a 24-well format by following calcium phosphate protocol. Briefly, 0.5 mL of SL2 cell suspension (at density of $0.5\text{-}1X10^6$ cells/mL) was plated into 24-well plates. After 24 h, cells were transfected with a mixture of 500 ng of shRNA construct and 200 ng PMT-Gal4 (for knockdown) or 500 ng of *Hy_pMT Laccase2_ circATP8B(2)* construct or empty vector. After 24h, cells were first treated with 25 μM $CuSO_4$ for 4–6 days (for knockdown) or 2 days (for overexpression) and subsequently infected by FHV (MOI 0.1), DCV (MOI 0.1) or CrPV (MOI 0.01) for indicated times. For expressing Flag-tagged proteins, various constructs were transfected into SL2 cells as described above. After 24h, cells were treated with 25 μM $CuSO_4$ for 2 days and expression of Flag-tagged protein was examined by immunoblot. To measure cell viability, cells were collected and washed in PBS. Subsequently, 6 μL cell suspension (~10000 cells) were incubated with 18 μL 0.04% Trypan Blue (Invitrogen, T10282) for 5 min at room temperature. Next 20 μL of the resultant cell/Trypan Blue mixture was loaded and cell viability was quantified using Cellometer Auto T4 (Nexcelom).

Plaque assays—Plaque assays were performed as the following.[61] Briefly, SL2 cells were seeded in 12-well plates and allowed to attach for 6–8 h. The medium was subsequently removed, and cells were incubated with 500 μL serum-free medium supplemented with diluted culture supernatants from infected cells containing virus for 1 h at room temperature. Next, cells were washed with PBS and coated with complete Schneider medium containing 1% low melting point agarose at room temperature for 48 h. Subsequently, cells were stained with 0.05% (w/v) crystal violet solution. Visible plaques were counted regardless of size and viral titer was calculated.

***Drosophila* infection and host survival—**Flies (4–7 d) were collected for viral infection experiment via injection. Glass needles were connected with an Nanoject II microinjection setup. About 4.6 nL RNA virus suspension (FHV: 1000 PFU/μL; DCV 2000 PFU/μL; CrPV:1000 PFU/μL) or sterile PBS was injected into each fly. After indicated times, flies were collected, and total RNA was isolated and subjected to RT-qPCR analysis to measure viral RNA load. To monitor host survival post viral infection, groups of 40 flies were infected and subsequently maintained at 25°C. Fly survival was monitored daily. Statistical significance was calculated with long rank test. Viral infection via oral feeding was performed as the following.[62,63] Flies of 4–7 d were first starved for 4 h. These flies were subsequently transferred to and kept in new vials containing RNA virus (viral suspension of $5X10^5$ $TCID_{50}$ units in 50 μL PBS containing blue dye (to monitor food consumption) was added to a filter paper disk that was placed on the surface of food) for 24h. Next, infected flies were transferred to and kept in vials containing regular food for indicated times. Fly gut tissue (10 per sample) was collected, total RNA was isolated and subjected to RT-qPCR analysis to measure levels of various viral and host RNAs. As for infection by *Ecc15*, 4–7 d flies were first starved for 4 h, and subsequently transferred to new food vials supplemented with a concentrated suspension of Ecc15 (OD_{600} = 20 in 50 μL PBS). Flies were collected 48 h post infection and rinsed in 70% ethanol to eliminate bacteria that are attached to the body surface. Subsequently, fly gut was collected and homogenized in sterile PBS. The homogenate was subjected to serial dilutions in sterile PBS, plated on LB-Amp plates and number of colonies were counted. Pathogen load was calculated and shown as cfu per fly. Each sample contains gut from 10 flies.

NAC feeding—Flies (4–7 d) were first starved 4 h and then transferred to and kept in food vials supplemented with 20 mM NAC or sterile PBS for 24 h. Flies were subsequently transferred to and kept in new vials containing various RNA viruses (viral suspension of $5X10^5$ $TCID_{50}$ units in 50 μL PBS was added to a filter paper disk that was placed on the food) for another 24 h. Infected flies were transferred to normal food vials and kept for indicated times. Fly gut tissue (5–10 fly gut per sample) was collected for RT-qPCR analysis or measurement of ROS levels.

Immunofluorescence assays—Gut tissue was dissected from female flies (with or without DCV infection via feeding) in PTN buffer (0.1 M sodium phosphate buffer, 0.1% Triton X-100) and fixed by 4% paraformaldehyde (Alfa Aesar, 43368) for 15 min at room temperature. After washing in PTN buffer for 3 times, 15 min each, samples were blocked with 5% BSA in PTN buffer at room temperature for 20 min and incubated with anti-Duox antibody (1:500, LSBio LS-C410118) or 4-HNE antibody (1:500, Abcam ab48506) at 4°C overnight. After washing in PTN buffer for 3 times, 15 min each, samples were incubated with secondary antibody (anti-Rabbit 594, 1:1000 or anti-mouse 594, 1:1000) at 4°C for 3h and washed in PTN buffer for 3 times. Samples were also counter-stained with DNA dye 4′,6′-diamidino-2-phenylindole (0.1 μg/mL DAPI in PBS) for 10 min. Subsequently, the samples were mounted in 80% glycerol and imaged by a Nikon confocal microscope (Nikon A1, Tokyo, Japan). The fluorescent density was quantified by ImageJ. For immunofluorescence assay in SL2 cells, cells were left uninfected or incubated in culture media containing viruses for 8 h. Cells were subsequently washed twice in PBS,

fixed in 4% paraformaldehyde for 10 min, washed 3 times in PTN, blocked by 5% BSA in PTN buffer at room temperature for 20 min, and incubated with anti-Duox antibody 4-HNE antibody at 4°C overnight. Cells were subsequently washed and incubated with secondary antibody (anti-Rabbit 594, 1:1000 or anti-mouse 594, 1:1000) for 1h at room temperature. Samples were also counter-stained with DNA dye 4′,6′-diamidino-2-phenylindole (0.1 μg/mL DAPI in PBS) for 10 min. The samples were then mounted in 80% glycerol and imaged by a Nikon confocal microscope (Nikon A1, Tokyo, Japan).

Immunoblot analysis—Cells were collected and lysed in lysis buffer (20 mM Tris-HCl (pH 7.6), 150 mM NaCl, 2 mM EDTA, 10% glycerol, 1% Triton X-100, 1 mM DTT, 1 mM orthovanadate) supplemented with protease inhibitor cocktail (Roche).[32] The samples were quantified by Pierce BCA Protein Assay Kit. Total lysates were loaded onto 10% SDS-PAGE, transferred to PVDF membrane, and subjected to immunoblot analysis using antibodies against FHV-B2 (1:2500) or Flag (Sigma, F7425, 1:5000).

RNA immunoprecipitation—To pull down the *circATP8B(2)*, a biotinylated oligo probe (Data S1) complementary to the back-spliced exon junction site of *circATP8B(2)* was designed.[64] A probe with sense sequence to the back-spliced exon junction serves as negative control. Briefly, ~1X10^8 cells stably transfected with pMT-Laccase2-*circATP8B(2)* were induced with 25 μM $CuSO_4$ for 72 h, and collected and washed in ice-cold PBS. Cells were lysed in 500 μL lysis buffer (20 mM Tris-HCl (pH 7.6), 150 mM NaCl, 2 mM EDTA, 10% glycerol, 1% Triton X-100, 1 mM DTT, 1 mM orthovanadate) supplemented with protease inhibitor cocktail (Roche) and RNasin (Promega). Cell lysate was centrifuged at 15000 rpm at 4°C for 10 min, and cleared supernatant was incubated with 5 μg oligo probe at room temperature for 2 h. Next, ~30 μL of Streptavidin C1 magnetic beads (Invitrogen 65001) were subsequently added and the lysate was incubated at room temperature for another 2 h. Beads were collected and washed 3 times in lysis buffer. To measure RNA levels, beads were resuspended with 300 μL 0.4M NaCl and 300 μL phenol/chloroform/isoamyl alcohol. After vortexing, the mixture was centrifuged at 15000 rpm at 4°C for 10 min, supernatant was transferred to new tube and 2.5 volume of ethanol was added to precipitate RNA. The resultant RNA was analyzed by RT-qPCR. To identify and analyze proteins that are enriched in the pulldown reaction, beads were also boiled in SDS loading buffer and subjected to immunoblot and/or mass spectrometry.

To preform RNA immunoprecipitation using protein as bait, ~1X10^8 SL2 cells were transfected with expression constructs for various Flag- or TAP-tagged proteins and subsequently induced with 25 μM $CuSO_4$ for 48 h. Cells were collected and lysed in 500 μL lysis buffer (20 mM Tris-HCl (pH 7.6), 150 mM NaCl, 2 mM EDTA, 10% glycerol, 1% Triton X-100, 1 mM DTT, 1 mM orthovanadate) supplemented with protease inhibitor cocktail (Roche) and RNasin (Promega). About 500 μL cleared total lysates were incubated with 20 μL anti-Flag beads (Sigma, A2220) or IgG Sepharose (GE healthcare, GE17-0969-01) at 4°C overnight. Subsequently, beads were washed 3 times in lysis buffer (without protease inhibitor cocktail), heated in SDS loading buffer, and analyzed by immunoblot. For RNA analysis, beads were resuspended with 300 μL 0.4M NaCl and 300 μL phenol/chloroform/isoamyl alcohol. After vortexing, the mixture was centrifuged at

15000 rpm at 4°C for 10 min, supernatant was transferred to new tube and 2.5 volume of ethanol was added to precipitate RNA. The resultant RNA was analyzed by RT-qPCR.

ROS assay—For measurement of ROS levels, fly gut tissue was dissected from 4 to 7 d female flies that were either left untreated or infected with DCV (5–10 fly gut per sample), or cells were collected and washed twice in PBS. Subsequently, the samples were lysed in lysis buffer. Protein concentration in cleared lysate were quantified using Pierce BCA Protein Assay Kit. For each sample, lysate containing 1 μg of protein was employed for ROS detection using the Fluorometric Hydrogen Peroxide Assay Kit (SIGMA) according to the manufacture's protocol.

RNase R treatment—RNase R treatment was performed as the following.[32,57] RNA samples were either left untreated or treated with RNase R at 37°C for 30 min. Subsequently, 2 μg of mouse total RNA was added to the samples and the samples were subjected to reverse transcription using Superscript III (Invitrogen). Levels of various circular and linear RNAs were measured by RT-qPCR using the iQ SYBR-green reagents on a CFX384 Real-Time PCR Detection System (Bio-Rad) and normalized against the mouse *gapdh* transcript. Fold changes in RNA levels were calculated using the ΔΔCt method.

QUANTIFICATION AND STATISTICAL ANALYSIS

p values for lifespan experiments were obtained by performing a log rank test. p values for RT-qPCR experiments were obtained by performing a two-tailed t test with multiple comparisons and correction for multiple tests on ΔΔCT values from at least three independent experiments. Visualization of data was performed in Prism 10 (Graphpad). The statistical parameters for experiments can be found in the figure legends, n indicates biological replicates. The number of animals used per experiment can be found in the method details section. Significance was defined as $p < 0.05$.

Supplementary Material

Refer to Web version on PubMed Central for supplementary material.

ACKNOWLEDGMENTS

We thank Dr. Neal Silverman for *Ecc15*, Dr. Jeremy Wilusz for the Hy_pMT-Laccase2-MCS-exon vector, Drs. Sara Cherry and Anette Schneemann for the anti-FHV B2 antibody, and BDSC for fly stocks. We thank members of the Zhou, Bhat, and Perera groups for advice and Hailey Hayes for technical support and helping with graphics and proofreading. This work was supported by NIH grants 1R01AI140049 and 1R21AI131099 (to R.Z.) and 1R01NS124668 and 1R03CA165184 (to R.J.P.), Florida Department of Health Bankhead-Coley Cancer Research Program grant 5BC08 (to R.J.P.), and the Sanford Burnham Prebys Medical Discovery Institute and Johns Hopkins University (to R.J.P. and R.Z.). J.L. is supported by the Intramural Research Program of the NIEHS/NIH.

REFERENCES

1. Hetru C, and Hoffmann JA (2009). NF-kappaB in the immune response of Drosophila. Cold Spring Harb. Perspect. Biol 1, a000232. 10.1101/cshperspect.a000232. [PubMed: 20457557]
2. Zhou R, Silverman N, Hong M, Liao DS, Chung Y, Chen ZJ, and Maniatis T (2005). The role of ubiquitination in Drosophila innate immunity. J. Biol. Chem 280, 34048–34055. 10.1074/jbc.M506655200. [PubMed: 16081424]

3. Silverman N, Zhou R, Erlich RL, Hunter M, Bernstein E, Schneider D, and Maniatis T (2003). Immune activation of NF-kappaB and JNK requires Drosophila TAK1. J. Biol. Chem 278, 48928–48934. 10.1074/jbc.M304802200. [PubMed: 14519762]
4. Silverman N, Zhou R, Stö ven S, Pandey N, Hultmark D, and Maniatis T (2000). A Drosophila IkappaB kinase complex required for Relish cleavage and antibacterial immunity. Genes Dev. 14, 2461–2471. [PubMed: 11018014]
5. Rutschmann S, Jung AC, Zhou R, Silverman N, Hoffmann JA, and Ferrandon D (2000). Role of Drosophila IKK gamma in a toll-independent antibacterial immune response. Nat. Immunol 1, 342–347. 10.1038/79801. [PubMed: 11017107]
6. Wang XH, Aliyari R, Li WX, Li HW, Kim K, Carthew R, Atkinson P, and Ding SW (2006). RNA interference directs innate immunity against viruses in adult Drosophila. Science 312, 452–454. 10.1126/science.1125694. [PubMed: 16556799]
7. van Rij RP, Saleh MC, Berry B, Foo C, Houk A, Antoniewski C, and Andino R (2006). The RNA silencing endonuclease Argonaute 2 mediates specific antiviral immunity in Drosophila melanogaster. Genes Dev. 20, 2985–2995. 10.1101/gad.1482006. [PubMed: 17079687]
8. Galiana-Arnoux D, Dostert C, Schneemann A, Hoffmann JA, and Imler JL (2006). Essential function in vivo for Dicer-2 in host defense against RNA viruses in drosophila. Nat. Immunol 7, 590–597. 10.1038/ni1335. [PubMed: 16554838]
9. Deddouche S, Matt N, Budd A, Mueller S, Kemp C, Galiana-Arnoux D, Dostert C, Antoniewski C, Hoffmann JA, and Imler JL (2008). The DExD/H-box helicase Dicer-2 mediates the induction of antiviral activity in drosophila. Nat. Immunol 9, 1425–1432. 10.1038/ni.1664. [PubMed: 18953338]
10. Xiong XP, Kurthkoti K, Chang KY, Lichinchi G, De N, Schneemann A, MacRae IJ, Rana TM, Perrimon N, and Zhou R (2013). Core small nuclear ribonucleoprotein particle splicing factor SmD1 modulates RNA interference in Drosophila. Proc. Natl. Acad. Sci. USA 110, 16520–16525. 10.1073/pnas.1315803110. [PubMed: 24067655]
11. Dostert C, Jouanguy E, Irving P, Troxler L, Galiana-Arnoux D, Hetru C, Hoffmann JA, and Imler JL (2005). The Jak-STAT signaling pathway is required but not sufficient for the antiviral response of drosophila. Nat. Immunol 6, 946–953. 10.1038/ni1237. [PubMed: 16086017]
12. Zambon RA, Nandakumar M, Vakharia VN, and Wu LP (2005). The Toll pathway is important for an antiviral response in Drosophila. Proc. Natl. Acad. Sci. USA 102, 7257–7262. 10.1073/pnas.0409181102. [PubMed: 15878994]
13. Holleufer A, Winther KG, Gad HH, Ai X, Chen Y, Li L, Wei Z, Deng H, Liu J, Frederiksen NA, et al. (2021). Two cGAS-like receptors induce antiviral immunity in Drosophila. Nature 597, 114–118. 10.1038/s41586-021-03800-z. [PubMed: 34261128]
14. Slavik KM, Morehouse BR, Ragucci AE, Zhou W, Ai X, Chen Y, Li L, Wei Z, Bähre H, König M, et al. (2021). cGAS-like receptors sense RNA and control 3’2’-cGAMP signalling in Drosophila. Nature 597, 109–113. 10.1038/s41586-021-03743-5. [PubMed: 34261127]
15. Nakamoto M, Moy RH, Xu J, Bambina S, Yasunaga A, Shelly SS, Gold B, and Cherry S (2012). Virus recognition by Toll-7 activates antiviral autophagy in Drosophila. Immunity 36, 658–667. 10.1016/j.immuni.2012.03.003. [PubMed: 22464169]
16. Liu Y, Gordesky-Gold B, Leney-Greene M, Weinbren NL, Tudor M, and Cherry S (2018). Inflammation-Induced, STING-Dependent Autophagy Restricts Zika Virus Infection in the Drosophila Brain. Cell Host Microbe 24, 57–68.e3. 10.1016/j.chom.2018.05.022. [PubMed: 29934091]
17. Molleston JM, Sabin LR, Moy RH, Menghani SV, Rausch K, Gordesky-Gold B, Hopkins KC, Zhou R, Jensen TH, Wilusz JE, and Cherry S (2016). A conserved virus-induced cytoplasmic TRAMP-like complex recruits the exosome to target viral RNA for degradation. Genes Dev. 30, 1658–1670. 10.1101/gad.284604.116. [PubMed: 27474443]
18. Ferreira ÁG, Naylor H, Esteves SS, Pais IS, Martins NE, and Teixeira L (2014). The Toll-dorsal pathway is required for resistance to viral oral infection in Drosophila. PLoS Pathog. 10, e1004507. 10.1371/journal.ppat.1004507. [PubMed: 25473839]
19. Mondotte JA, Gausson V, Frangeul L, Blanc H, Lambrechts L, and Saleh MC (2018). Immune priming and clearance of orally acquired RNA viruses in Drosophila. Nat. Microbiol 3, 1394–1403. 10.1038/s41564-018-0265-9. [PubMed: 30374170]

20. Wong ZS, Brownlie JC, and Johnson KN (2015). Oxidative stress correlates with Wolbachia-mediated antiviral protection in Wolbachia-Drosophila associations. Appl. Environ. Microbiol 81, 3001–3005. 10.1128/AEM.03847-14. [PubMed: 25710364]
21. Xiong XP, Kurthkoti K, Chang KY, Li JL, Ren X, Ni JQ, Rana TM, and Zhou R (2016). miR-34 Modulates Innate Immunity and Ecdysone Signaling in Drosophila. PLoS Pathog. 12, e1006034. 10.1371/journal.ppat.1006034. [PubMed: 27893816]
22. O'Connell RM, Rao DS, and Baltimore D (2012;30:295–312). MicroRNA Regulation of Inflammatory Responses. Annu. Rev. Immunol 10.1146/annurev-immunol-020711-075013. [PubMed: 22224773]
23. Cai X, Schäfer A, Lu S, Bilello JP, Desrosiers RC, Edwards R, Raab-Traub N, and Cullen BR (2006). Epstein-Barr virus microRNAs are evolutionarily conserved and differentially expressed. PLoS Pathog. 2, e23. 10.1371/journal.ppat.0020023. [PubMed: 16557291]
24. Cook HL, Lytle JR, Mischo HE, Li MJ, Rossi JJ, Silva DP, Desrosiers RC, and Steitz JA (2005). Small nuclear RNAs encoded by Herpesvirus saimiri upregulate the expression of genes linked to T cell activation in virally transformed T cells. Curr. Biol 15, 974–979. 10.1016/j.cub.2005.04.034. [PubMed: 15916956]
25. Lee N, Yario TA, Gao JS, and Steitz JA (2016). EBV noncoding RNA EBER2 interacts with host RNA-binding proteins to regulate viral gene expression. Proc. Natl. Acad. Sci. USA 113, 3221–3226. 10.1073/pnas.1601773113. [PubMed: 26951683]
26. Salzman J, Chen RE, Olsen MN, Wang PL, and Brown PO (2013). Cell-type specific features of circular RNA expression. PLoS Genet. 9, e1003777. 10.1371/journal.pgen.1003777. [PubMed: 24039610]
27. Salzman J, Gawad C, Wang PL, Lacayo N, and Brown PO (2012). Circular RNAs are the predominant transcript isoform from hundreds of human genes in diverse cell types. PLoS One 7, e30733. 10.1371/journal.pone.0030733. [PubMed: 22319583]
28. Memczak S, Jens M, Elefsinioti A, Torti F, Krueger J, Rybak A, Maier L, Mackowiak SD, Gregersen LH, Munschauer M, et al. (2013). Circular RNAs are a large class of animal RNAs with regulatory potency. Nature 495, 333–338. 10.1038/nature11928. [PubMed: 23446348]
29. Guo JU, Agarwal V, Guo H, and Bartel DP (2014). Expanded identification and characterization of mammalian circular RNAs. Genome Biol. 15, 409. 10.1186/s13059-014-0409-z. [PubMed: 25070500]
30. Hansen TB, Jensen TI, Clausen BH, Bramsen JB, Finsen B, Damgaard CK, and Kjems J (2013). Natural RNA circles function as efficient microRNA sponges. Nature 495, 384–388. 10.1038/nature11993. [PubMed: 23446346]
31. Liu W, Liang W, Xiong XP, Li JL, and Zhou R (2022). A circular RNA Edis-Relish-castor axis regulates neuronal development in Drosophila. PLoS Genet. 18, e1010433. 10.1371/journal.pgen.1010433. [PubMed: 36301831]
32. Xiong XP, Liang W, Liu W, Xu S, Li JL, Tito A, Situ J, Martinez D, Wu C, Perera RJ, et al. (2022). The Circular RNA Edis Regulates Neurodevelopment and Innate Immunity. PLoS Genet. 18, e1010429. 10.1371/journal.pgen.1010429. [PubMed: 36301822]
33. Liu CX, Li X, Nan F, Jiang S, Gao X, Guo SK, Xue W, Cui Y, Dong K, Ding H, et al. (2019). Structure and Degradation of Circular RNAs Regulate PKR Activation in Innate Immunity. Cell 177, 865–880.e21. 10.1016/j.cell.2019.03.046. [PubMed: 31031002]
34. Ha EM, Oh CT, Bae YS, and Lee WJ (2005). A direct role for dual oxidase in Drosophila gut immunity. Science 310, 847–850. 10.1126/science.1117311. [PubMed: 16272120]
35. Ha EM, Lee KA, Park SH, Kim SH, Nam HJ, Lee HY, Kang D, and Lee WJ (2009). Regulation of DUOX by the Galphaq-phospholipase Cbeta-Ca2+ pathway in Drosophila gut immunity. Dev. Cell 16, 386–397.10.1016/j.devcel.2008.12.015. [PubMed: 19289084]
36. Jeck WR, Sorrentino JA, Wang K, Slevin MK, Burd CE, Liu J, Marzluff WF, and Sharpless NE (2013). Circular RNAs are abundant, conserved, and associated with ALU repeats. RNA 19, 141–157. 10.1261/rna.035667.112. [PubMed: 23249747]
37. Houseley JM, Garcia-Casado Z, Pascual M, Paricio N, O'Dell KMC, Monckton DG, and Artero RD (2006). Noncanonical RNAs from transcripts of the Drosophila muscleblind gene. J. Hered 97, 253–260. 10.1093/jhered/esj037. [PubMed: 16714427]

38. Petrillo JE, Venter PA, Short JR, Gopal R, Deddouche S, Lamiable O, Imler JL, and Schneemann A (2013). Cytoplasmic granule formation and translational inhibition of nodaviral RNAs in the absence of the double-stranded RNA binding protein B2. J. Virol 87, 13409–13421. 10.1128/JVI.02362-13. [PubMed: 24089564]
39. Cao C, Cogni R, Barbier V, and Jiggins FM (2017). Complex Coding and Regulatory Polymorphisms in a Restriction Factor Determine the Susceptibility of Drosophila to Viral Infection. Genetics 206, 2159–2173. 10.1534/genetics.117.201970. [PubMed: 28630113]
40. Costa A, Jan E, Sarnow P, and Schneider D (2009). The Imd pathway is involved in antiviral immune responses in Drosophila. PLoS One 4, e7436. 10.1371/journal.pone.0007436. [PubMed: 19829691]
41. Ha EM, Oh CT, Ryu JH, Bae YS, Kang SW, Jang IH, Brey PT, and Lee WJ (2005). An antioxidant system required for host protection against gut infection in Drosophila. Dev. Cell 8, 125–132. 10.1016/j.devcel.2004.11.007. [PubMed: 15621536]
42. Li X, Rommelaere S, Kondo S, and Lemaitre B (2020). Renal Purge of Hemolymphatic Lipids Prevents the Accumulation of ROS-Induced Inflammatory Oxidized Lipids and Protects Drosophila from Tissue Damage. Immunity 52, 374–387.e6. 10.1016/j.immuni.2020.01.008. [PubMed: 32075729]
43. Basset A, Khush RS, Braun A, Gardan L, Boccard F, Hoffmann JA, and Lemaitre B (2000). The phytopathogenic bacteria Erwinia carotovora infects Drosophila and activates an immune response. Proc. Natl. Acad. Sci. USA 97, 3376–3381. 10.1073/pnas.97.7.3376. [PubMed: 10725405]
44. Zafarullah M, Li WQ, Sylvester J, and Ahmad M (2003). Molecular mechanisms of N-acetylcysteine actions. Cell. Mol. Life Sci 60, 6–20. 10.1007/s000180300001. [PubMed: 12613655]
45. Piwecka M, Glažar P, Hernandez-Miranda LR, Memczak S, Wolf SA, Rybak-Wolf A, Filipchyk A, Klironomos F, Cerda Jara CA, Fenske P, et al. (2017). Loss of a mammalian circular RNA locus causes miRNA deregulation and affects brain function. Science 357, eaam8526. 10.1126/science.aam8526. [PubMed: 28798046]
46. Legnini I, Di Timoteo G, Rossi F, Morlando M, Briganti F, Sthandier O, Fatica A, Santini T, Andronache A, Wade M, et al. (2017). Circ-ZNF609 Is a Circular RNA that Can Be Translated and Functions in Myogenesis. Mol. Cell 66, 22–37.e9. 10.1016/j.molcel.2017.02.017. [PubMed: 28344082]
47. Pamudurti NR, Bartok O, Jens M, Ashwal-Fluss R, Stottmeister C, Ruhe L, Hanan M, Wyler E, Perez-Hernandez D, Ramberger E, et al. (2017). Translation of CircRNAs. Mol. Cell 66, 9–21.e7. 10.1016/j.molcel.2017.02.021. [PubMed: 28344080]
48. Ashwal-Fluss R, Meyer M, Pamudurti NR, Ivanov A, Bartok O, Hanan M, Evantal N, Memczak S, Rajewsky N, and Kadener S (2014). circRNA biogenesis competes with pre-mRNA splicing. Mol. Cell 56, 55–66. 10.1016/j.molcel.2014.08.019. [PubMed: 25242144]
49. Schnall-Levin M, Zhao Y, Perrimon N, and Berger B (2010). Conserved microRNA targeting in Drosophila is as widespread in coding regions as in 3'UTRs. Proc. Natl. Acad. Sci. USA 107, 15751–15756. 10.1073/pnas.1006172107. [PubMed: 20729470]
50. Zuker M (2003). Mfold web server for nucleic acid folding and hybridization prediction. Nucleic Acids Res. 31, 3406–3415. 10.1093/nar/gkg595. [PubMed: 12824337]
51. Castello A, Fischer B, Eichelbaum K, Horos R, Beckmann BM, Strein C, Davey NE, Humphreys DT, Preiss T, Steinmetz LM, et al. (2012). Insights into RNA biology from an atlas of mammalian mRNA-binding proteins. Cell 149, 1393–1406. 10.1016/j.cell.2012.04.031. [PubMed: 22658674]
52. Kramer MC, Liang D, Tatomer DC, Gold B, March ZM, Cherry S, and Wilusz JE (2015). Combinatorial control of Drosophila circular RNA expression by intronic repeats, hnRNPs, and SR proteins. Genes Dev. 29, 2168–2182. 10.1101/gad.270421.115. [PubMed: 26450910]
53. Langmead B, and Salzberg SL (2012). Fast gapped-read alignment with Bowtie 2. Nat. Methods 9, 357–359. 10.1038/nmeth.1923. [PubMed: 22388286]
54. Dobin A, Davis CA, Schlesinger F, Drenkow J, Zaleski C, Jha S, Batut P, Chaisson M, and Gingeras TR (2013). STAR: ultrafast universal RNA-seq aligner. Bioinformatics 29, 15–21. 10.1093/bioinformatics/bts635. [PubMed: 23104886]

55. Liao Y, Smyth GK, and Shi W (2014). featureCounts: an efficient general purpose program for assigning sequence reads to genomic features. Bioinformatics 30, 923–930. 10.1093/bioinformatics/btt656. [PubMed: 24227677]

56. McCarthy DJ, Chen Y, and Smyth GK (2012). Differential expression analysis of multifactor RNA-Seq experiments with respect to biological variation. Nucleic Acids Res. 40, 4288–4297. 10.1093/nar/gks042. [PubMed: 22287627]

57. Rybak-Wolf A, Stottmeister C, Glažar P, Jens M, Pino N, Giusti S, Hanan M, Behm M, Bartok O, Ashwal-Fluss R, et al. (2015). Circular RNAs in the Mammalian Brain Are Highly Abundant, Conserved, and Dynamically Expressed. Mol. Cell 58, 870–885. 10.1016/j.molcel.2015.03.027. [PubMed: 25921068]

58. Zhou R, Hotta I, Denli AM, Hong P, Perrimon N, and Hannon GJ (2008). Comparative analysis of argonaute-dependent small RNA pathways in Drosophila. Mol. Cell 32, 592–599. 10.1016/j.molcel.2008.10.018. [PubMed: 19026789]

59. Zhou R, Mohr S, Hannon GJ, and Perrimon N (2013). Inducing RNAi in Drosophila cells by transfection with dsRNA. Cold Spring Harb. Protoc 2013, 461–463. 10.1101/pdb.prot074351. [PubMed: 23637371]

60. Zhou R, Mohr S, Hannon GJ, and Perrimon N (2014). Inducing RNAi in Drosophila cells by soaking with dsRNA. Cold Spring Harb. Protoc 2014, pdb.prot080747. 10.1101/pdb.prot080747.

61. Scotti PD (1977). End-point dilution and plaque assay methods for titration of cricket paralysis virus in cultured Drosophila cells. J. Gen. Virol 35, 393–396. 10.1099/0022-1317-35-2-393. [PubMed: 406358]

62. Xu J, Hopkins K, Sabin L, Yasunaga A, Subramanian H, Lamborn I, Gordesky-Gold B, and Cherry S (2013). ERK signaling couples nutrient status to antiviral defense in the insect gut. Proc. Natl. Acad. Sci. USA 110, 15025–15030. 10.1073/pnas.1303193110. [PubMed: 23980175]

63. Sansone CL, Cohen J, Yasunaga A, Xu J, Osborn G, Subramanian H, Gold B, Buchon N, and Cherry S (2015). Microbiota-Dependent Priming of Antiviral Intestinal Immunity in Drosophila. Cell Host Microbe 18, 571–581. 10.1016/j.chom.2015.10.010. [PubMed: 26567510]

64. Du WW, Yang W, Liu E, Yang Z, Dhaliwal P, and Yang BB (2016). Foxo3 circular RNA retards cell cycle progression via forming ternary complexes with p21 and CDK2. Nucleic Acids Res. 44, 2846–2858. 10.1093/nar/gkw027. [PubMed: 26861625]

Highlights

- *circATP8B(2)* depletion *in vivo* or in cells enhances antiviral defense in *Drosophila*
- *circATP8B(2)* depletion in fly gut impairs oral viral infection
- *circATP8B(2)* binds to and inhibits the activity of the ROS-producing enzyme Duox
- *circATP8B(2)* modulates *Duox* expression and Duox-dependent ROS production

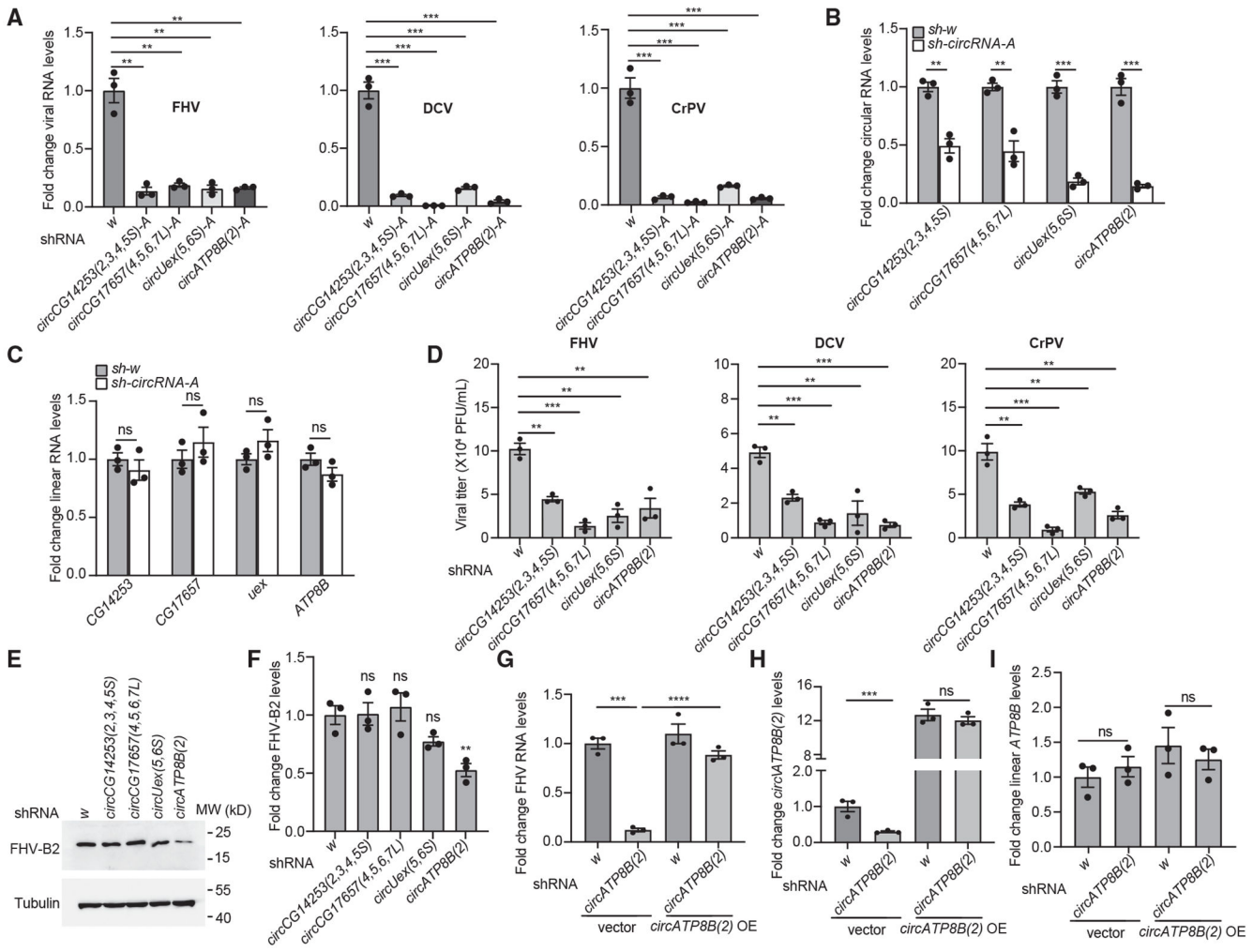

Figure 1. Depletion of select circRNAs compromises viral RNA replication in SL2 cells

(A–C) SL2 cells stably transfected with shRNA constructs (*shRNA-A*) targeting the back-spliced exon junction of select circRNAs or a control shRNA targeting *white* (*w*) were first treated with 25 μM $CuSO_4$ for 4 days. Subsequently, cells were either left untreated or infected with FHV (MOI 0.1), DCV (MOI 0.1), or CrPV (MOI 0.01) for 8 h. Levels of FHV RNA1, DCV, and CrPV RNAs (A) and various circRNAs (B) and linear RNAs (C) were measured by RT-qPCR and normalized to control *Rp49* (n = 3).

(D) A similar set of cells as in (A) was infected with FHV (MOI 0.1), DCV (MOI 0.1), or CrPV (MOI 0.01). Cell culture medium was collected, and viral titer was determined by plaque assay (n = 3).

(E and F) A similar set of cells as in (A) was infected with FHV for 8 h (MOI 0.1). Cell lysates were loaded on parallel gels, and levels of FHV-B2 protein (top) and tubulin (bottom, control) were measured by immunoblot (E) and quantified in (F) (n = 3).

(G–I) Restoring *circATP8B(2)* expression in *circATP8B(2)*-depleted cells rescues the viral RNA replication phenotype. SL2 cells were transfected with shRNA targeting *circATP8B(2)* or a control shRNA together with a Gal4 expression vector driven by the *metallothionein* promoter and empty vector or *circATP8B(2)* overexpression constructs. Cells were first

treated with 25 μM $CuSO_4$ for 4 days. Subsequently, cells were treated with FHV for 8 h (MOI 0.1). Levels of FHV RNA (G), *circATP8B(2)* (H), and linear *ATP8B* (I) were measured (n = 3).

All RT-PCR data in this paper are presented as mean + standard error of the mean (SEM). *p < 0.05, **p < 0.01, ***p < 0.001; ns, non-significant.

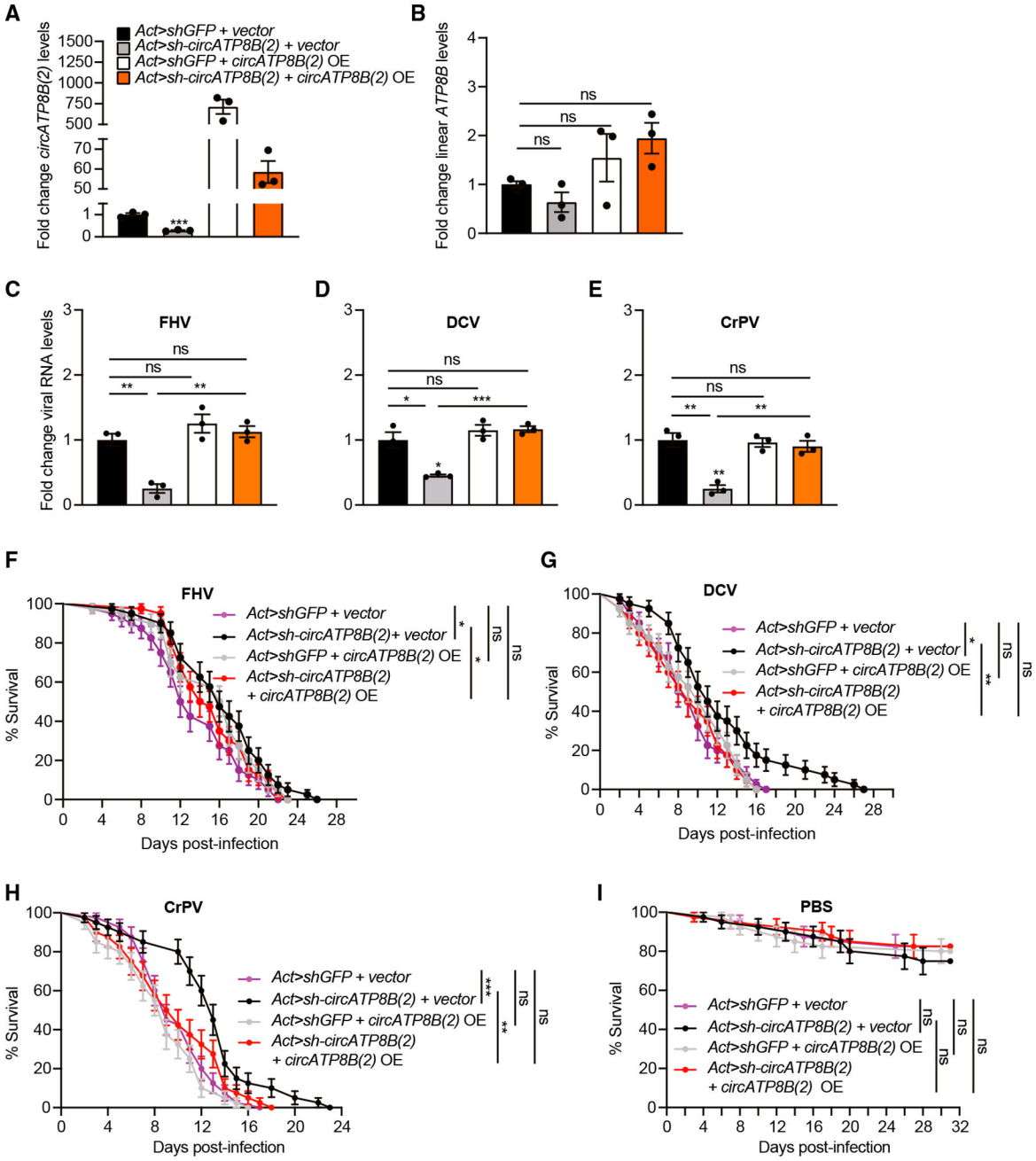

Figure 2. Ubiquitous depletion of *circATP8B(2) in vivo* compromises virus infection

(A–E) Flies carrying the *Act-Gal4* driver were crossed to *UAS-sh-circATP8B(2)* or control *UAS-sh-GFP* flies together with the empty vector or *circATP8B(2)* overexpression (OE) transgenes. Female progeny of the indicated genotypes was injected with various viruses and collected for RT-PCR analysis 48 h post infection. Levels of *circATP8B(2)* (A), linear *ATP8B* (B), and various viral RNAs (C–E) were measured (10 files per group as one biological replicate, n = 3).

(F–I) Female progeny of the indicated genotypes was injected with FHV (F), DCV (G), CrPV (H), or sterile PBS (I), and survival was measured post infection. For each genotype, 40 flies were analyzed. Survival data are presented as mean + standard error (SE). *$p < 0.05$, **$p < 0.01$, ***$p < 0.001$.

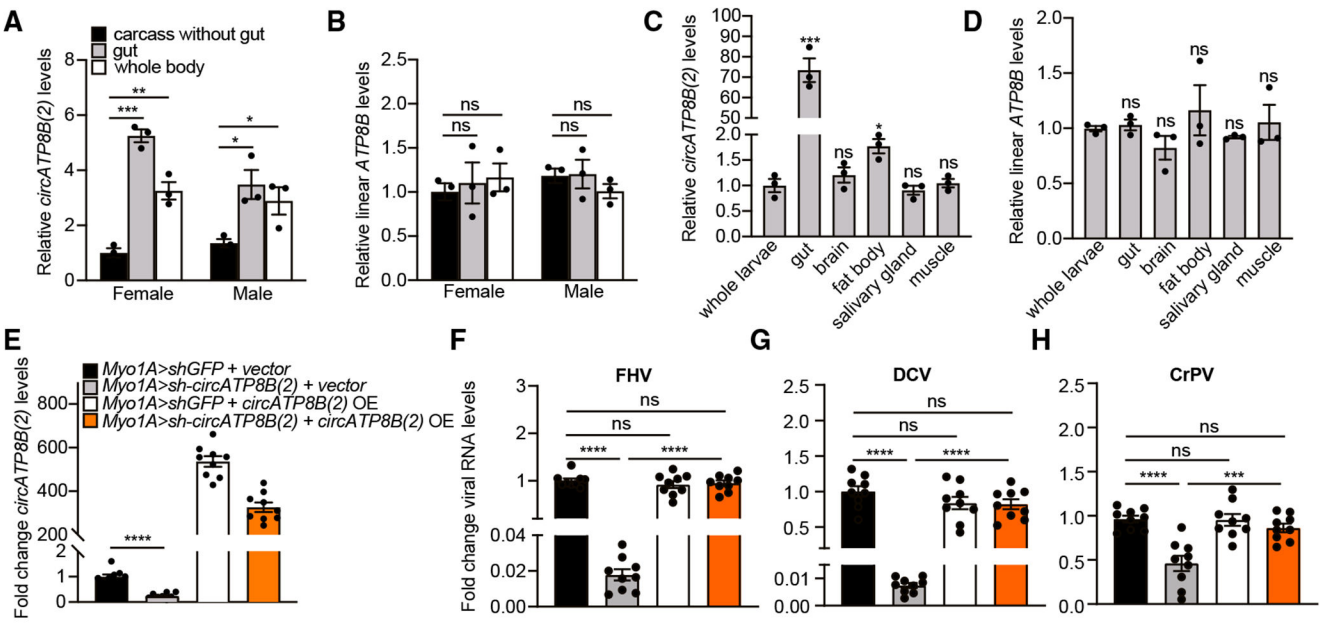

Figure 3. *circATP8B(2)* is enriched in the gut and impacts oral viral infection

(A–D) Total RNAs were extracted from whole adult fly, fly gut, and fly carcasses without gut (A and B) or whole larvae and various larval tissues/organs (C and D, gut, brain, fat body, salivary gland, muscle). Levels of *circATP8B(2)* (A and C) and linear *ATP8B* (B and D) RNAs are shown (n = 3).

(E–H) Flies carrying the gut-specific *Myo1A-Gal4* driver were crossed to U*AS-sh-circATP8B(2)* or control *UAS-sh-GFP* flies together with the empty vector or *circATP8B(2)* OE transgenes. Female progeny of the indicated genotypes was pre-starved for 4 h and then fed with various viruses for 24 h: FHV (F), DCV (G), or CrPV (H). Flies were subsequently transferred to clean food vials and kept for another 48 h. Total RNA was extracted from fly gut and levels of *circATP8B(2)* (E) and various viral RNAs were measured by RT-PCR: FHV (F), DCV (G), or CrPV (H) (10 guts per biological replicate, n = 9).

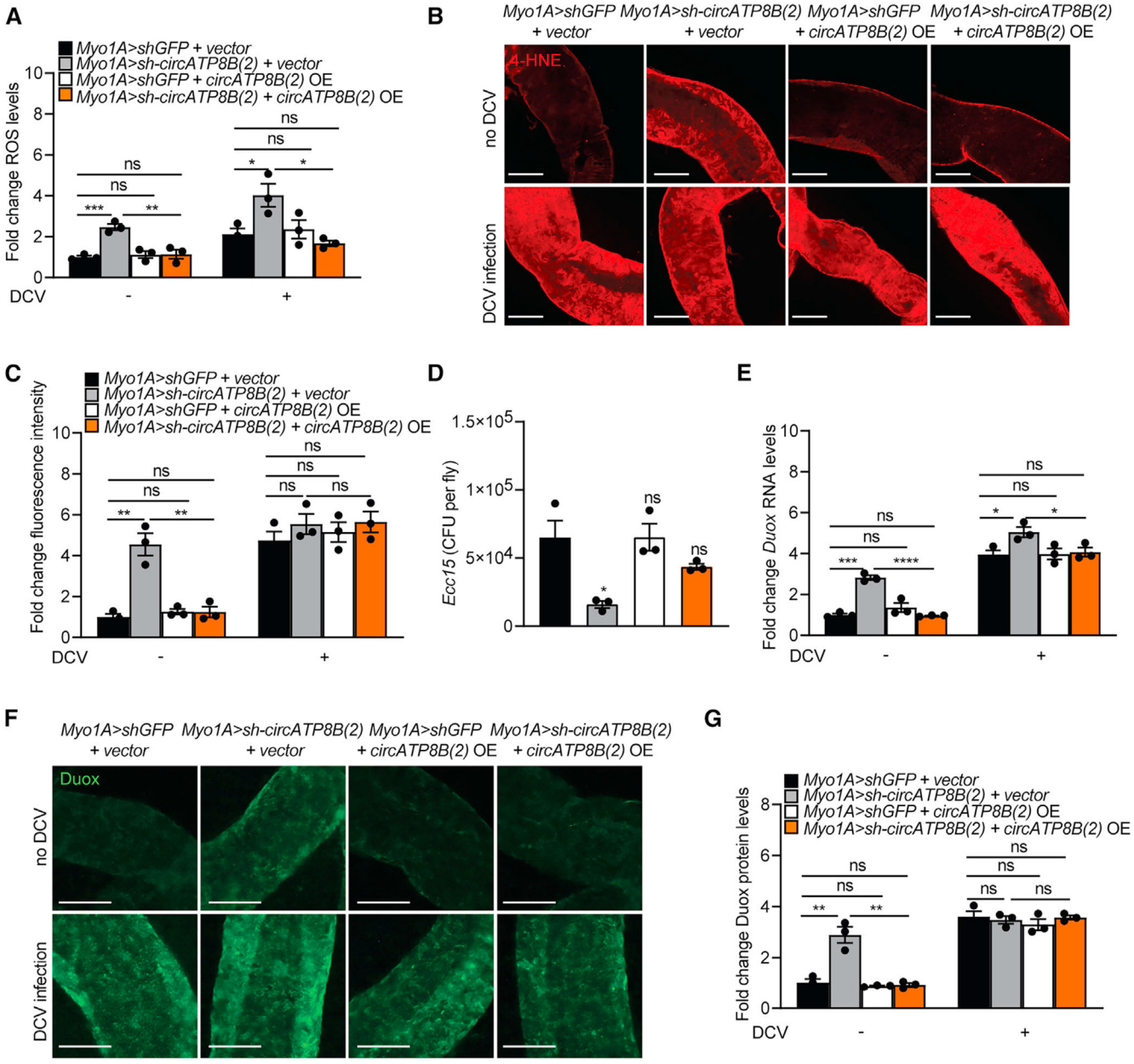

Figure 4. Depletion of *circATP8B(2)* in the fly gut leads to upregulation of *Duox* expression and elevated ROS levels

(A–C) Depletion of *circATP8B(2)* in the fly gut leads to elevated ROS levels. Female progeny of the indicated genotypes was pre-starved for 4 h and then fed with DCV or sterile PBS (non-infected) for 24 h. Flies were subsequently transferred to clean food vials. Fly gut was collected after 48 h, and levels of ROS were measured (A, n = 3). In addition, a similar set of samples as in (A) was collected and subjected to an immunofluorescence assay using an anti-4-HNE antibody (B; scale bars, 50 μm), and the relative fluorescence intensity was quantified (C) (n = 3).

(D) Female progeny of the same genotypes as in (A) was fed with *Ecc15* for 48 h. Gut tissue from groups of 10 flies was collected and homogenized. Pathogen load was measured and is shown as colony-forming units (CFUs) per fly (n = 3).

(E–G) Depletion of *circATP8B(2)* in the fly gut leads to upregulation of *Duox* expression. A similar set of samples as in (A) was collected. Total RNA was extracted, and levels of *Duox* transcript were measured by RT-PCR and normalized to the control *Rp49* (E, n = 3). In addition, another set of samples was subjected to an immunofluorescence assay using an anti-Duox antibody (F; scale bars, 50 μm), and the relative fluorescence intensity was quantified (G) (n = 3).

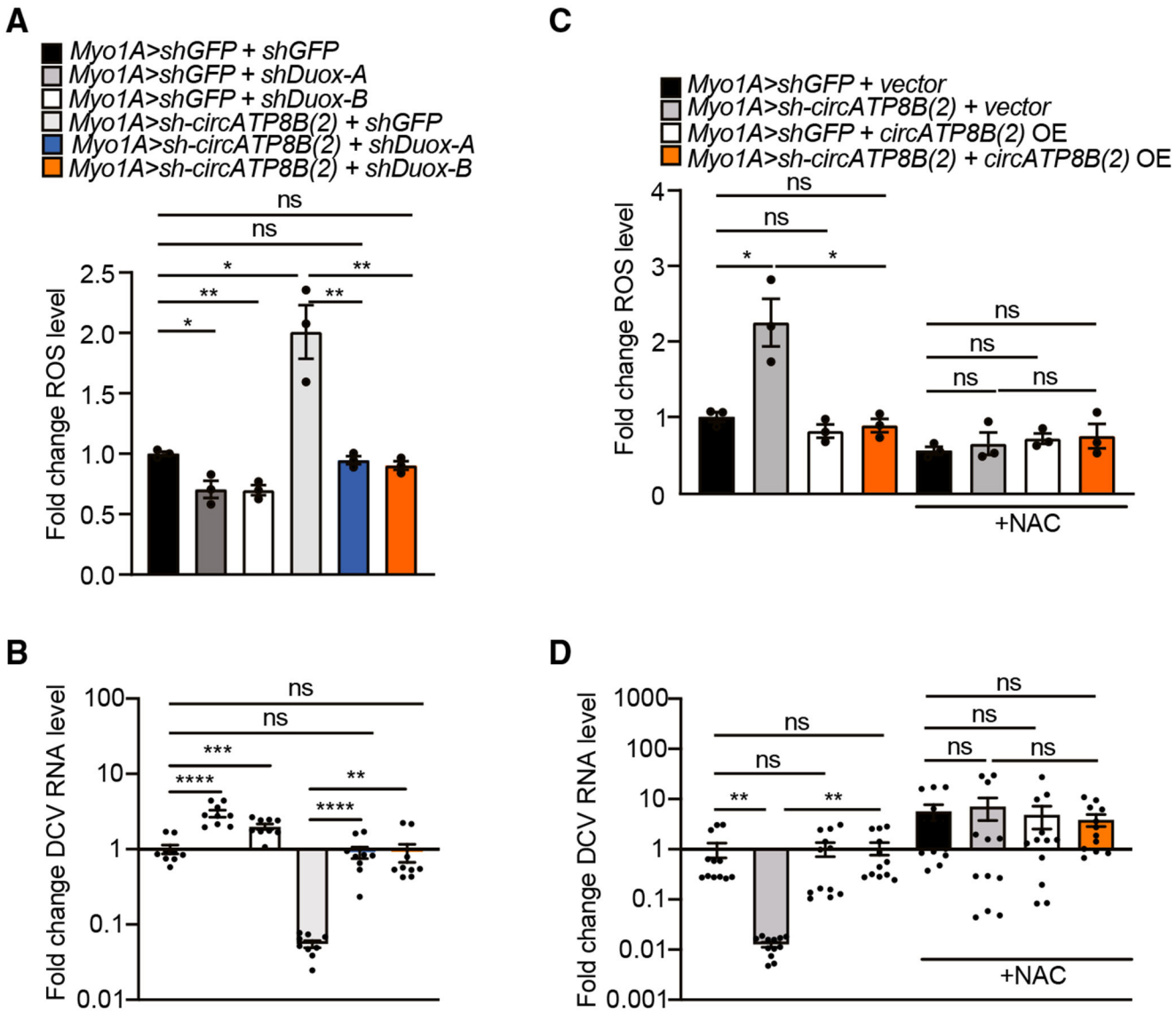

Figure 5. Reducing ROS levels in the fly gut rescues the viral RNA replication phenotype elicited by *circATP8B(2)* depletion

(A and B) Depletion of *Duox* rescues the viral RNA replication phenotype and reduces ROS levels in *circATP8B(2)*-depleted flies. Female progeny of the indicated genotypes was pre-starved for 4 h and then fed with DCV for 24 h. Flies were subsequently transferred to clean food vials. Gut tissue from a group of 10 flies was collected after 48 h, and levels of ROS were measured (A) (n = 3). In addition, total RNA was extracted from gut tissue from a group of 10 flies, and levels of viral RNA were measured by RT-qPCR and normalized to *Rp49* (B) (n = 9).

(C and D) NAC-mediated removal of ROS from the fly gut rescues the viral RNA replication phenotype elicited by *circATP8B(2)* depletion. Female progeny of the indicated genotypes was first starved overnight and then fed for 24 h with food supplemented with or without 20 mM ROS inhibitor N-acetyl-l-cysteine (NAC). Flies were subsequently fed with DCV

for 24 h and transferred to regular food for 48 h. Gut tissue (from 10 flies per sample) was collected. Levels of ROS were measured (C) (n = 3). In addition, total RNA was extracted, and levels of viral RNA were measured by RT-qPCR and normalized to *Rp49* (D) (n = 12).

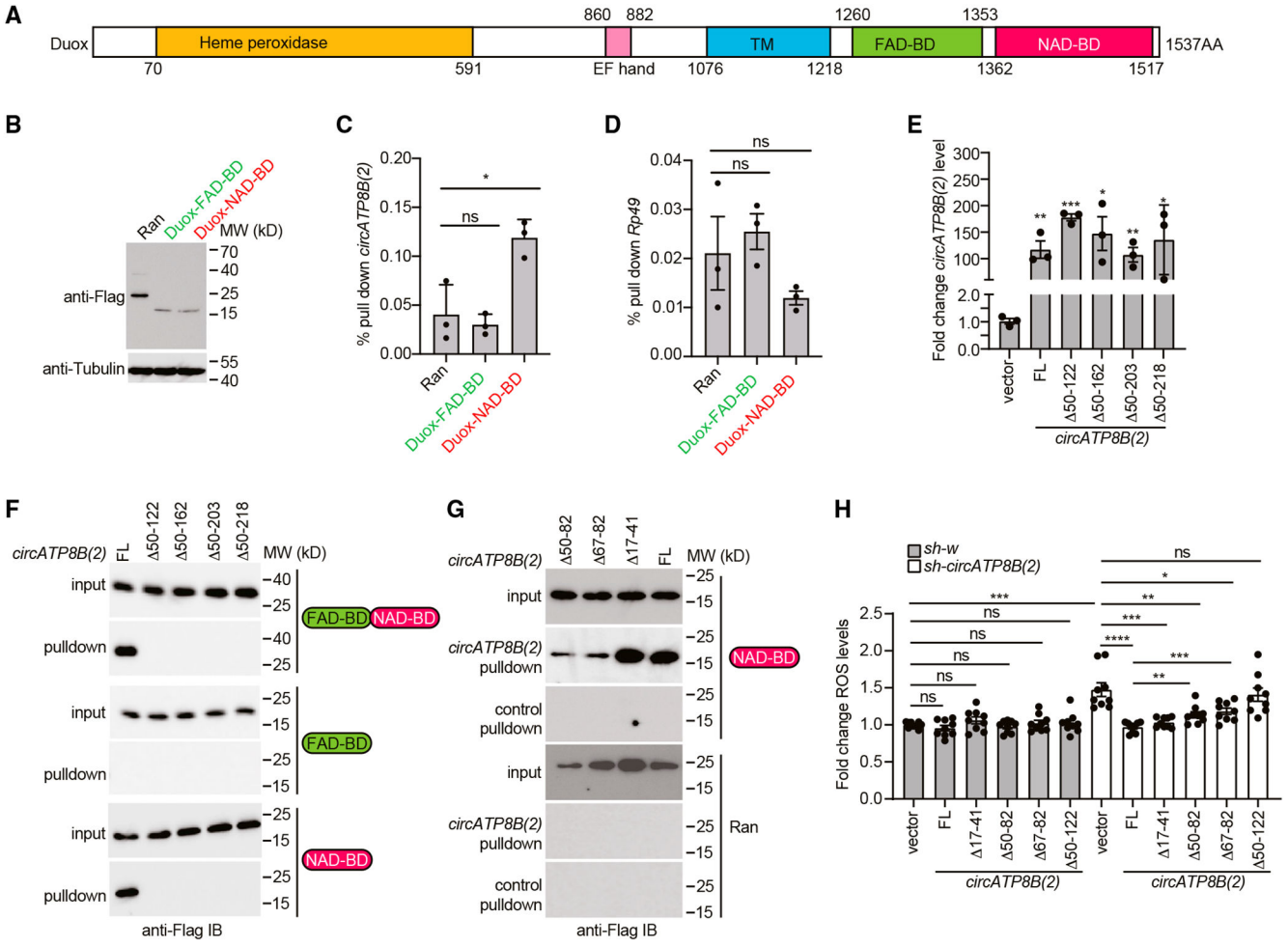

Figure 6. *circATP8B(2)* interacts with Duox

(A) A schematic of Duox showing various domains, including a peroxidase homology domain, an EF hand domain, a transmembrane (TM) domain, a FAD-BD, and a NAD-BD. (B–D) FLAG-tagged FAD-BD, NAD-BD of Duox, or the control protein Ran was expressed in SL2 cells. Cells were collected, and cell lysates were analyzed by immunoblot to detect various FLAG-tagged proteins and tubulin (B). In addition, cell lysates were subjected to immunoprecipitation using anti-FLAG antibody. Total RNA was extracted from immune-purified anti-FLAG complexes, and levels of *circATP8B(2)* (C) and control *Rp49* (D) were measured by RT-qPCR (n = 3). The percentage of pull-down relative to input samples is shown.

(E—G) FLAG-tagged Duox C-terminal fragments (FAD-BD, NAD-BD, or FAD-BD+NAD-BD) and the control protein Ran were expressed in SL2 cells together with full-length or truncated *circATP8B(2)* mutants. Comparable levels of *circATP8B(2)* were detected in various samples as measured by RT-qPCR (E, n = 3). *circATP8B(2)*-containing complexes were pulled down using a biotinylated DNA oligo complementary to the back-spliced exon junction and subjected to immunoblot to detect FLAG-tagged proteins (F and G). A control pull-down using a biotinylated DNA oligo with a sense sequence to the back-spliced exon junction of *circATP8B(2)* served as a negative control.

(H) Full-length or various truncational mutants of *circATP8B(2)* or empty vector were transfected to SL2 cells stably expressing a control shRNA (*sh-w*) or *sh-circATP8B(2)*. Cells were harvested, and levels of ROS were measured (n = 9).

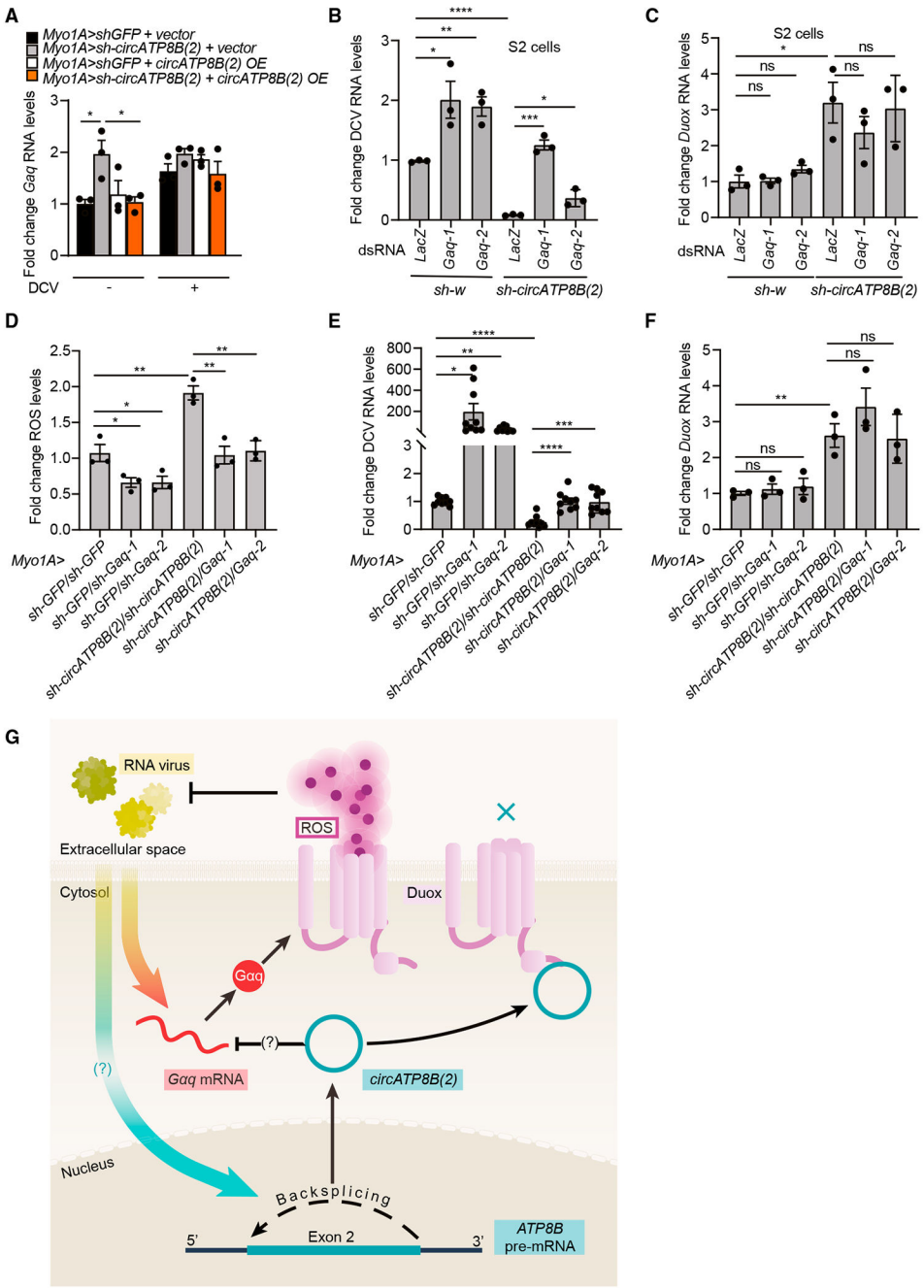

Figure 7. Gaq acts downstream of *circATP8B(2)* to regulate Duox activity

(A) Levels of *Gaq* transcript are elevated upon *circATP8B(2)* depletion. Flies of the indicated genotypes were left infected or fed with DCV, and levels of *Gaq* transcript in the fly gut were measured by RT-qPCR and normalized to control *Rp49* (n = 3).

(B and C) S2 cells stably transfected with a control shRNA (*sh-w*) or *sh-circATP8B(2)* were treated with various dsRNAs and subsequently infected with DCV. Levels of DCV (B) and *Duox* RNA (C) were measured (n = 3).

(D–F) Flies of the indicated genotypes were fed with DCV, and levels of ROS (D), DCV (E), and Duox RNA (F) in the fly gut were measured (n = 3–9).

(G) *circATP8B(2)*-mediated regulation of Duox-dependent ROS production and antiviral defense.

KEY RESOURCES TABLE

REAGENT or RESOURCE	SOURCE	IDENTIFIER
Antibodies		
FHV B2	Anette Schneemann (Petrillo et al.)[38]	N/A
Duox	LSBio	Cat#LS-C410118
4-HNE	Abcam	Cat#ab48506; RRID:AB_867452
anti-Rabbit 594	Fisher Scientific	Cat#A-21207; RRID:AB_141637
anti-mouse 594	Fisher Scientific	Cat# A-11005; RRID:AB_2534073
Flag	Sigma	Cat#F7425; RRID:AB_439687
anti-mouse IgG-HRP	Fisher Scientific	Cat#31430; RRID:AB_228307
anti-Rabbit-IgG-HRP	Fisher Scientific	Cat#31460; RRID:AB_228341
Bacterial and virus strains		
Drosophila C virus	Anette Schneemann	RRID:NCBITaxon_64279
Flock House Virus	Anette Schneemann	RRID:NCBITaxon_12287
Cricket paralysis virus	Anette Schneemann	RRID:NCBITaxon_12136
Ecc15	Neal Silverman (Basset et al.)[43]	N/A
Chemicals, peptides, and recombinant proteins		
FD&C Blue Dye #1	Spectrum Chemical	Cat#FD110-25GM; CAS# 3844-45-9
N-acetyl-L-cysteine	Fisher Scientific	Cat#AAA1540914; CAS616-91-1
RNasin	Promega	Cat#N2515
RNase R	Lucigen	Cat#RNR07250
Streptavidin C1 magnetic beads	Invitrogen	Cat#65001
anti-Flag M2 beads	Sigma	Cat#A2220
Critical commercial assays		
SuperScript III cDNA synthesis kit	Invitrogen	Cat#18080044
iQ SYBR Green Supermix	Bio-Rad	Cat#1708880
Fluorometric Hydrogen Peroxide Assay Kit	SIGMA	Cat#MAK165
Pierce™ BCA Protein Assay Kit	Fisher	Cat#23227
Deposited data		
RNA-seq	This paper	GSE248666 (https://www.ncbi.nlm.nih.gov/geo/query/acc.cgi?acc=GSE248666)
Experimental models: Cell lines		
D. melanogaster: Cell line S2: S2-DRSC	Laboratory of Norbert Perrimon	FlyBase: FBtc0000181
Experimental models: Organisms/strains		
D. melanogaster: Act-Gal4	Bloomington Drosophila Stock Center	FBst0004414; RRID:BDSC_4414
D. melanogaster: Myo1A-Gal4	Bloomington Drosophila Stock Center	FBtp0098092; RRID:BDSC_67057
D. melanogaster: sh-GFP	N. Perrimon (Harvard Medical School, Boston, MA)	N/A

REAGENT or RESOURCE	SOURCE	IDENTIFIER
D. melanogaster: sh-circATP8B(2): y v sc; +/+; UAS-sh-circATP8B(2)-A/TM3	This paper	N/A
D. melanogaster: sh-circATP8B(2): y v sc; +/+; UAS-sh-circATP8B(2)-B/TM3	This paper	N/A
D. melanogaster: UAS-circATP8B(2): w; UAS-laccase2-circATP8B(2)/CyO	This paper	N/A
D. melanogaster: UAS-laccase2-vector: w; UAS-laccase2-vector/CyO	This paper	N/A
D. melanogaster: Duox RNAi: y[1] sc[*] v[1] sev[21]; P{y[+t7.7] v[+t1.8] = TRiP.HMS00934}attP2	Bloomington Drosophila Stock Center	FBti0140636; RRID:BDSC_33975
D. melanogaster: Duox RNAi: y[1] sc[*] v[1] sev[21]; P{y[+t7.7] v[+t1.8] = TRiP.HMS00692}attP2	Bloomington Drosophila Stock Center	FBti0140406; RRID:BDSC_32903
D. melanogaster: Gaq RNAi: y[1] v[1]; P{y[+t7.7] v[+t1.8] = TRiP.JF02464}attP2	Bloomington Drosophila Stock Center	FBti0141010; RRID:BDSC_33765
D. melanogaster: Gaq RNAi: y[1] v[1]; P{y[+t7.7] v[+t1.8] = TRiP.JF02390}attP2	Bloomington Drosophila Stock Center	FBti0146822; RRID:BDSC_36775
D. melanogaster: ATP8B RNAi: y[1] v[1]; P{y[+t7.7] v[+t1.8] = TRiP.HMS05311}attP40	Bloomington Drosophila Stock Center	FBti0180114; RRID:BDSC_63037
D. melanogaster: LysC RNAi: y[1] sc[*] v[1] sev[21]; P{y[+t7.7] v[+t1.8] = TRiP.HMC05564}attP40	Bloomington Drosophila Stock Center	FBti0183793; RRID:BDSC_64545
D. melanogaster: Mdr49 RNAi: y[1] sc[*] v[1] sev[21]; P{y[+t7.7] v[+t1.8] = TRiP.HMS00400}attP2	Bloomington Drosophila Stock Center	FBti0132100; RRID:BDSC_32405
D. melanogaster: Nep7 RNAi: y[1] sc[*] v[1] sev[21]; P{y[+t7.7] v[+t1.8] = TRiP.HMS01076}attP2	Bloomington Drosophila Stock Center	FBti0140771; RRID:BDSC_34531
Oligonucleotides		
See Data S1		N/A
Recombinant DNA		
Hy_pMT Laccase2 MCS exon vector	Jeremy Wilusz (Kramer et al.)[52]	RRID:Addgene_69884
Hy_pMT Laccase2-circATP8B(2)	This paper	N/A
Hy_pMT Laccase2-circATP8B(2)-Δ50-122	This paper	N/A
Hy_pMT Laccase2-circATP8B(2)-Δ17-41	This paper	N/A
Hy_pMT Laccase2-circATP8B(2)-Δ50-82	This paper	N/A
Hy_pMT Laccase2-circATP8B(2)-Δ67-82	This paper	N/A
pRmHa-3-Flag Duox FAD-BD + NAD-BD	This paper	N/A
pRmHa-3-Flag Duox FAD-BD	This paper	N/A
pRmHa-3-Flag Duox NAD-BD	This paper	N/A
pRmHa-3-Flag Ran	This paper	N/A
pRmHa-3-Flag endoG	This paper	N/A
pRmHa-3-Flag pEBP1	This paper	N/A
UAST Laccase2-circATP8B(2)	This paper	N/A
Valium 20-sh-circATP8B(2)-A	This paper	N/A
Valium 20-sh-circATP8B(2)-B	This paper	N/A
Software and algorithms		
bowtie2	Langmead and Salzberg[53]	https://bowtie-bio.sourceforge.net/bowtie2/index.shtml

REAGENT or RESOURCE	SOURCE	IDENTIFIER
find_circ	Memczak et al.[28]	N/A
STAR	Dobin et al.[54]	https://github.com/alexdobin/STAR
Subread	Liao et al.[55]	https://subread.sourceforge.net/
edgeR	McCarthy et al.[56]	https://bioconductor.org/packages/release/bioc/html/edgeR.html
M-Fold	Zuker[50]	http://www.unafold.org/mfold/applications/rna-folding-form.php
Graphpad Prism 10	Graphpad	https://www.graphpad.com